AN ABSTRACT OF THE THESIS OF

Jimson S. Lounsbury for the degree of Master of Science in Electrical and Computer Engineering presented on January 4, 2012.

Title: Distributed Temperature Sensing with Neodymium-Doped Optical Fiber

Abstract approved:

Thomas K. Plant

Polymer electrolyte membrane (PEM) fuel cells are being studied for use as high efficiency power plants in alternative fuel vehicles. To maintain high efficiency the operating temperatures of the membranes in these fuel cells must be closely monitored and controlled. However, the environment inside of the fuel cell is not favorable for traditional temperature sensing, so a new optical-fiber-based, distributed temperature sensor was proposed to address this need.

This thesis investigates the properties of neodymium-doped optical fiber for use as a distributed temperature sensor for PEM fuel cells. The optical absorption spectrum was measured to identify the energy band structure and determine upconversion excitation schemes. The temperature coefficient of the Nd^{3+}-doped silica fiber fluorescence decay time was measured for several bands of emission. Finally, two-photon upconversion was attempted from the lower excited states of Nd:YAG and Nd:silica.

Distributed Temperature Sensing with Neodymium-Doped Optical Fiber

by
Jimson S. Lounsbury

A THESIS

submitted to

Oregon State University

In partial fulfillment of
the requirements for the
degree of

Master of Science

Presented January 4, 2012
Commencement June 2012

Master of Science thesis of Jimson S. Lounsbury presented on January 4, 2011.

APPROVED:

Major Professor, representing Electrical and Computer Engineering

---

Director of the School of Electrical Engineering and Computer Science

---

Dean of the Graduate School

I understand that my thesis will become part of the permanent collection of Oregon State University libraries. My signature below authorizes release of my thesis to any reader upon request.

Jimson S. Lounsbury, Author

TABLE OF CONTENTS

1 Introduction 1

2 Background and Previous Work 4

2.1 Remote Temperature Sensing Introduction 4

2.2 Temperature Sensing with Phosphors 6

2.3 Techniques with Optical Fibers 11

2.4 Proposed Sensing Scheme 14

3 Nd^{3+}-doped fiber spectroscopy 19

3.1 Introduction to Neodymium Spectroscopy 19

3.2 Absorption Spectra 19

3.3 Fluorescence Spectra 29

4 Fluorescence Temperature Dependent Behavior 34

4.1 Experimental Setup 35

4.2 Results 38

5 Two-Photon Upconversion from Lower Excited States of Nd-doped hosts 44

6 Conclusions and Future Work 51

7 Bibliography 55

LIST OF FIGURES

Figure Page

Figure 2-1: Simple two-level energy band diagram..... 7

Figure 2-2: Configurational coordinate model..... 9

Figure 2-3: Two-photon distributed sensor scheme..... 15

Figure 2-4: Simple energy band diagram for two-photon sensing scheme..... 16

Figure 2-5: Nd3+ energy band diagram showing typical excitation process with key energy level assignments..... 17

Figure 2-6: Nd3+ energy band diagram showing proposed excitation process with key energy level assignments..... 18

Figure 3-1: Cross-section of Nd-doped double clad fiber from Nufern..... 20

Figure 3-2: Experimental setup for optical absorption spectra 22

Figure 3-3: Relative detector response curves 22

Figure 3-4: 0.03% Nd-doped fiber optical absorption spectrum for upper energy states 25

Figure 3-5: Optical absorption spectra for Nd:glass, Nd:YAG, and Nd:silica 26

Figure 3-6: $^4I_{15/2}$ absorption band in Nd:silica (0.03% concentration), Nd:YAG, Nd:glass..... 27

Figure 3-7: $^4I_{15/2}$ Absorption Band in Nd:Silica (0.5% concentration), Nd:YAG, Nd:glass..... 28

Figure 3-8: Experimental setup for Nd-doped optical fiber fluorescence spectroscopy 29

Figure 3-9: Nd:silica fluorescence bands..... 31

Figure 3-10: Fluorescence spectra of Nd:silica, Nd:YAG, and Nd:glass 31

LIST OF FIGURES (Continued)

Figure Page

Figure 3-11: Nd:silica fluorescence in optical with and without cladding modes 33

Figure 4-1: Temperature-dependent fluorescence lifetime in Nd:YAG (1.064 μm) ... 34

Figure 4-2: Picture of fiber sample being optically excited in oven 36

Figure 4-3: Fluorescence decay from pulsed excitation in Nd-doped optical fiber 37

Figure 4-4: Temperature dependent fluorescence decay time constant for 908 nm emission 39

Figure 4-5: Temperature dependent fluorescence decay time constant for 940 nm emission 40

Figure 4-6: Temperature dependent fluorescence decay time constant for 1090 nm emission 40

Figure 4-7: Temperature dependence of fluorescence amplitude 41

Figure 4-8: Quantum efficiencies of different semiconductors 43

Figure 5-1: Optical absorption band for $^4I_{15/2}$ energy level in Nd:YAG 46

Figure 5-2: Diagram of sample setup for upconversion experiment..... 47

Distributed Temperature Sensing with

Neodymium-Doped Optical Fiber

1 Introduction

In 2003 the Department of Energy began sponsoring research in the development of all aspects of a hydrogen fuel cell vehicle: fuel generation, storage, energy conversion, motor, drive, efficiency, environmental impact, etc. The project was called the FreedomCAR. One of the fuel cell technologies to be explored in the project was the Polymer Electrolyte Membrane Fuel Cell (PEMFC). The PEMFC has the potential to be an extremely efficient, low temperature, (safe), hydrogen fuel cell. The heart of a PEMFC is the membrane itself.

The anode of the fuel cell contains a catalyst which strips away the electrons from the protons in the H_2 molecule, while allowing only the protons to be transported across the membrane. On the cathode side, the protons and electrons, which have now done electrical work, combine with O_2 to form liquid H_2O. The liquid H_2O which forms does double duty by keeping the membrane moist and aiding the proton exchange across the membrane. For this process to work efficiently, PEMs need to be maintained in a tightly controlled temperature range. If the PEM is run at too low a temperature or too high a temperature, the process is not efficient and may not be viable in a vehicle. The membranes need to be maintained at a temperature close to

100 ºC to operate efficiently. To maintain this operating condition for maximum efficiency, active feedback for the fuel cell membrane is required.

The environment within the fuel cell is quite hostile due to the presence of liquid water as well as an electric current. This type of environment is not compatible with traditional electrical-based remote temperature sensors. This fact led to an investigation of the use of optical-fiber-based temperature sensors for this application.

S.W. Allison and others at Oak Ridge National Laboratories (ORNL) began demonstrating that a thermographic phosphor-tipped optical fiber could be used to effectively probe a PEMFC. However, this approach is limited because it only measures the temperature in a single discrete location. Ideally, the temperature gradient across the membrane could be monitored. They proposed that designing a fast distributed temperature sensor (DTS) with high spatial resolution would be the next step. It was proposed that a rare-earth-doped optical fiber would be a good candidate to be integrated into the fuel cell, eventually leading to waveguides integrated into the membrane itself. If an array of these types of sensors were integrated into the fuel cell, this would make it possible to monitor the membrane temperature throughout the fuel cell. Toward this goal, S.W. Allison and T.K. Plant proposed the study of a neodymium-doped optical fiber as a possible early candidate for a high resolution distributed sensor scheme.

Chapter 2 of this thesis reviews relevant literature focusing on rare earth and optical fiber temperature sensing. Additionally, it includes a description of the proposed sensing scheme. Chapter 3 describes the experimental setups for the

spectroscopy of the Nd^{3+}-doped optical fiber, and discusses the findings. Chapter 4 details the results from the temperature-dependent fluorescent time decay experiments of the sample. Chapter 5 describes the investigation to find two-photon upconversion from the lower excited states in Nd^{3+}. Chapter 6 presents the conclusions, as well as recommendations for future research in distributed optical fiber temperature sensors.

2 Background and Previous Work

2.1 Remote Temperature Sensing Introduction

Many modern day systems require temperature monitoring to maintain process controls in order to maximize efficiency. For instance, at various points in a modern automobile engine, temperature is monitored to ensure that it runs at peak efficiency and performance. To this end, temperature sensors like thermocouples, thermistors, and platinum resistance temperature detectors (RTD), the cousin to the thermistor, are classic choices when monitoring temperature in a process. All of these types of sensors are well studied and have been commercially available for a long time.

In the case of the thermocouple, the thermoelectric effect in dissimilar metals was discovered nearly two hundred years ago, in 1821, by Thomas Seebeck. The Seebeck effect, as it is known, was characterized for a whole host of metal combinations. If we look at the first order approximation of this effect, equation 1.1, we see that for a change in the temperature of the junction (ΔT), there will be a proportional change in the voltage (ΔV) across the junction, according to the Seebeck coefficient (S) for that particular type of junction.

$$\Delta V = S \times \Delta T \tag{1.1}$$

This relationship makes this type of device very compatible with electric circuits and somewhat easy to integrate with modern process controllers. The coefficients for common junction types, however, are less than 100 μV/ºC. This is a significant drawback because thermocouples are leaded devices and must be

connected to the metal conductors in a voltmeter and this means they will have at least two junctions of dissimilar metals per sensor. This extra junction can be dealt with by controlling its temperature and creating a reference point. This reference point is referred to as the ice point because it was historically set by using an ice bath. Since this is not practical in many situations an electronic ice point is typically used. Generating an electronic ice point usually requires a voltage reference, tunable resistor network, and a thermistor. While thermocouples typically work over a larger overall temperature range than thermistors, high precision measurements in this case will require heavy averaging of the measurement and require significant additional instrumentation for absolute measurement accuracy.

Thermistors and RTDs are both sensors whose electrical resistance varies with temperature. Thermistors are typically ceramic or polymer-based and their properties depend on the fabrication process, not on the material's elemental material properties. RTDs are metal-based, but still depend on the fabrication process to achieve the final device properties. This means that their properties can be tailored and optimized for their application. If we look at the first order approximation for the thermistor response this time, the change in resistance (ΔR) of the device is proportional to the change in temperature (ΔT) multiplied by a temperature coefficient of resistance constant C.

$$\Delta R = C \times \Delta T \tag{1.2}$$

A simple voltage divider circuit can be used with this type of device, usually achieving a response better than 1 mV/ºC. This means they are more sensitive than

thermocouples over their relatively limited operating temperature range. This, combined with the fact that a thermistor is a passive circuit element, means that they are a favorite in embedded circuit designs.

While the thermocouple and the thermistor have been mainstay sensors since the beginning of remote temperature sensing, they do have limitations in the environments in which they can be used. Harsher environments, which can be explosive, corrosive, or even smaller than the physical dimensions of a thermistor or thermocouple element, will not be able to accommodate these types of sensors. These types of environments necessitate the use of other types of sensors.

2.2 Temperature Sensing with Phosphors

The study of thermographic phosphors began in the late 1930's and was sparked by the invention of the fluorescent lamp. It wasn't until the last 20 years or so that they moved into a more practical role, due to the need for high speed optical sources and instrumentation. Fluorescing phosphors are typically defined as a white or slightly colored powder which is made up of an inert crystalline or glass host material, and an "activating" impurity which will emit its own light when excited with ultraviolet or visible light. The phosphors can be shaped or deposited in a number of ways and then applied to the substrate of interest. Once applied, the phosphors are in thermal equilibrium with the substrate. The phosphor is then optically excited and the temperature-dependent fluorescence is measured to determine the temperature of the

substrate. The phosphor can be deposited or bound to an object in some way and not requiring any other infrastructure to the substrate of interest. This allows a non-contact measurement to be made without any wires to the substrate allowing it to move freely and even rotate.

The emitted light from a fluorescing phosphor will typically have a decay time constant, which is temperature dependent for many phosphors. The nature of the temperature-dependent decay of the excited emission can be partially described with the simple two-level energy band diagram shown in Figure 2-1.

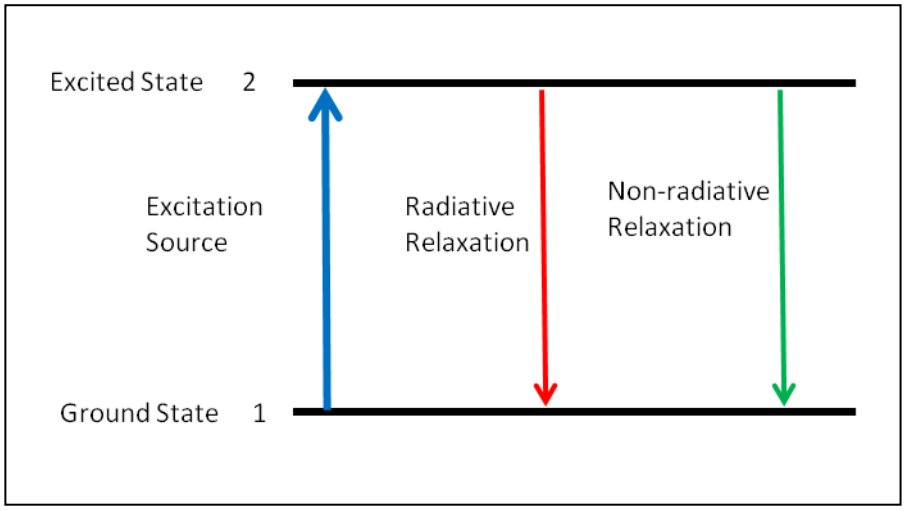

Figure 2-1: Simple two-level energy band diagram

The transition rate from the excited to the ground state is described as the sum of rates of the spontaneous radiative emission A, which is constant, and a non-radiative component W whose magnitude is temperature dependent[1].

$$k = \frac{1}{\tau} = A_{1,2} + W_{1,2} \tag{2.1}$$

The exact make-up of the non-radiative component will depend on both the doping concentration of the active rare-earth elements and also the specific host material. It may be assumed that the non-radiative process is dominated by random thermally generated atomic vibrations if the doping concentration is not so high that there is direct energy transfer between ions. As an example, Grattan and Zhang[2] describe this process for Cr^{3+} in $LiSrAlF_6$ but whose principle applies generally in other materials as well, such as in Nd:YAG[3]. In this example the overall transition rate $\frac{1}{\tau}$ is described by equation 2.2, below,

$$\frac{1}{\tau} = \frac{1}{\tau_i} + \left(\frac{1}{\tau_q}\right) e^{\frac{-\Delta E_q}{kT}} \tag{2.2}$$

where τ_i is the intrinsic radiative lifetime; τ_q is the phonon relaxation time constant; ΔE_q is the thermal energy needed for a phonon to get to the ground state-excited state crossing point Q in the configurational coordinate model from Grattan is shown in Figure 2-2; k is the Boltzmann constant; and T is the temperature in degrees Kelvin.

From this diagram, we can see that there will be two observed temperature dependent effects on the fluorescence emission. The first is described by equation 2.2, which shows that as the material rises in temperature, the excited electrons will be promoted even higher. This makes it more likely that they will have the needed energy and momentum to couple into other non-radiative phonon relaxation processes.

These phonon processes will likely have a different transition decay time constant than the radiative transition and will affect the overall observed decay time constant. In this example, the phonon process was faster, so with increasing temperature, the overall observed decay time constant decreased with temperature. Likewise, we can also see that, since more of the excited electrons will follow non-radiative phonon processes with increased temperature, it follows that the overall amplitude of the material fluorescence will trend down with increasing temperature as well.

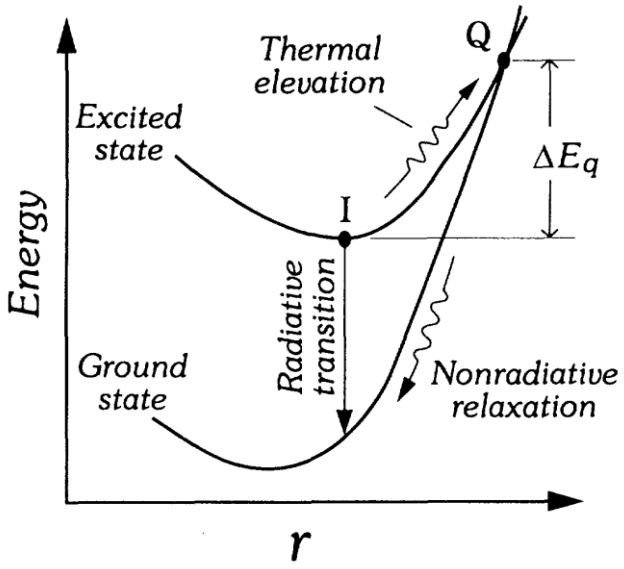

Figure 2-2: Configurational coordinate model

The expression then in equation 2.2 describes how this material can be used to measure temperature by way of the observed fluorescence decay time. This is a real advantage when measuring the temperature of moving or rotating objects since it is difficult to use traditional wired sensors in these situations. Grattan and Zhang are

also able to expand on equation 2.2 by using conservation of energy to show that the total observed fluorescence with a given excited state population will follow the relationship in equation 2.3. This means that it should be expected that the overall radiated emission intensity I should decrease with increasing temperature from its initial value I_0 (at T = 0 °K).

$$I = \frac{I_o}{1 + \left(\frac{\tau_i}{\tau_q}\right) e^{\frac{-\Delta E_q}{kT}}} \tag{2.3}$$

A third temperature-dependent characteristic of phosphor fluorescence that can be leveraged to make a sensor is the temperature-sensitive nature of the radiative spectrum of some materials. This effect will often manifest itself as a temperature-sensitive radiative branching ratio in the energy level fine structure as one radiative transition becomes preferred over another [5,13,15]. This effect is usually quite small and so is less suited as a high resolution temperature sensor.

The temperature-dependent effects described above make thermographic phosphors viable, and the nature of phosphors give them some important advantages over electrically conductive sensors when probing harsh environments. Because the phosphors are optically activated, the sensors can be extremely small, even just a thin coating evaporated onto the object being measured. They are also not subject to electromagnetic interference in particularly noisy environments; the measurement instrumentation can be far removed from the object being measured. The phosphors need only an optical path to receive the excitation pump and transmit the signal. This

is often done using a small phosphor element on the end of a waveguide. But it can also use a free space optical path, allowing the sensor to freely move and to not be tethered.

Despite these key advantages, phosphor sensors do have some fundamental limitations as well. First among these is the need for a "line of sight" optical path. Due to this limitation it was a natural step to begin attaching phosphors to the ends of optical fibers and use the optical waveguides as the conduit for the probe and signal. The advantages of this type of sensor, though, are still based on the same advantages of the phosphor sensor itself. This then leads us to the topic of optical fiber thermography.

Thermographic optical fibers fall into two main categories; extrinsic and intrinsic. The previous example is an extrinsic optical fiber temperature sensor (OFTS). The extrinsic optical fiber sensor will always couple an "active" sensor of some other technology to an optical fiber used simply as a waveguide. The intrinsic OFTS uses the temperature sensitive properties of the fiber itself as the sensing mechanism. This thesis will focus on the intrinsic type.

2.3 Techniques with Optical Fibers

Intrinsic OFTS is not a new area of study. In fact, it has been employed successfully for a number of applications where distributed temperature sensing

combined with the natural flexibility of optical fibers provide an advantage. Dr. John Selker, at Oregon State University, employed a distributed temperature sensor (DTS) to measure stream temperature dynamics and the geology of mountain groundwater movement[6]. This is an example of an application that highlights the singular unique capability of fiber optic thermometry; truly distributed temperature sensing.

Distributed intrinsic OFTSs have tremendous advantages over traditional temperature sensors. Since they are glass fibers, they can be made to withstand extreme environments; high and low temperatures, water, corrosive gases, etc. Optical fibers are immune to EMI, so signal integrity is maintained in electrically noisy environments. The fibers are inherently safe, with no electrical signals, so they can be used in explosive gas environments. Since a distributed sensor can measure all along its length, the sensor footprint and signal processing overhead is minimized, compared to what an array of point sensors would require for the same measurement capability.

There are two main types of fibers used in thermographic optical fiber sensing; undoped fibers, which rely on the properties of the silica glass fiber itself, and doped fibers, which rely on the properties of a rare earth dopant. For undoped fibers, a number of novel devices have been demonstrated using various properties of fibers: Rayleigh scatter, polarization, as well as non-linear Brillouin and Raman scattering.

An example of a device based on Brillouin scattering was demonstrated by Bao *et al.*[10]. In that case, the temperature sensitive nature of stimulated Brillouin scattering was employed to create a 22 km long DTS with 1°C temperature resolution. As is typical with sensors that depend on the non-linear properties of the fiber, fine

spatial resolution of the temperature along the fiber is usually challenging to achieve. In this case it was reported that a resolution of 10 meters was achieved. The magnitude of the wavelength shift of the Brillouin scatter is mapped to a corresponding shift in temperature. At the same time, the timing of the backscattered pulses indicates the location along the fiber where the measurement was made. This system requires both an optical time domain reflectometer (OTDR) and a spectrometer to simultaneously make this measurement. This type of measurement is typical for the non-linear scatter-based methods in that they must resolve the magnitude of the spectral shifts to resolve temperature.

In contrast, actively doped optical fiber DTS's rely on linear processes and typically have been demonstrated using the temperature dependent nature of the absorption spectra. Farries et al.[11] demonstrated this sort of device on a neodymium doped fiber. They demonstrated a spatial resolution of 15 meters with a temperature accuracy of 2°C.

As is common with all optical fiber DTS techniques, the primary method for interrogating spatial information is with an OTDR. The OTDR sends out a series of pulses in one end of the fiber and measures the time it takes to receive small back-scattered reflections of those pulses. The scatter can be Rayleigh, Raman, or Brillouin-based scatter. From the signal timing, the attenuation or gross changes in the optical fiber properties can be estimated. For this reason, all DTS techniques rely on extremely small signals for both their spatial and thermal information. The heavy

signal processing required to measure these small signals reduces the spatial resolution of the system.

2.4 Proposed Sensing Scheme

In this thesis, a neodymium-doped optical fiber is investigated for suitability in a novel DTS. This new scheme would not use the OTDR. Instead it would entail using the timing of two laser pulses of different optical frequencies traveling in opposite directions in the fiber. These pulses, when overlapping, would excite the fiber in a discrete location, causing the fiber to fluoresce in only that location. The fluorescence would then travel down the fiber in both directions and can then be interrogated for temperature information. This concept, proposed by S.W. Allison et. al.[12] , is illustrated in Figure 2-3.

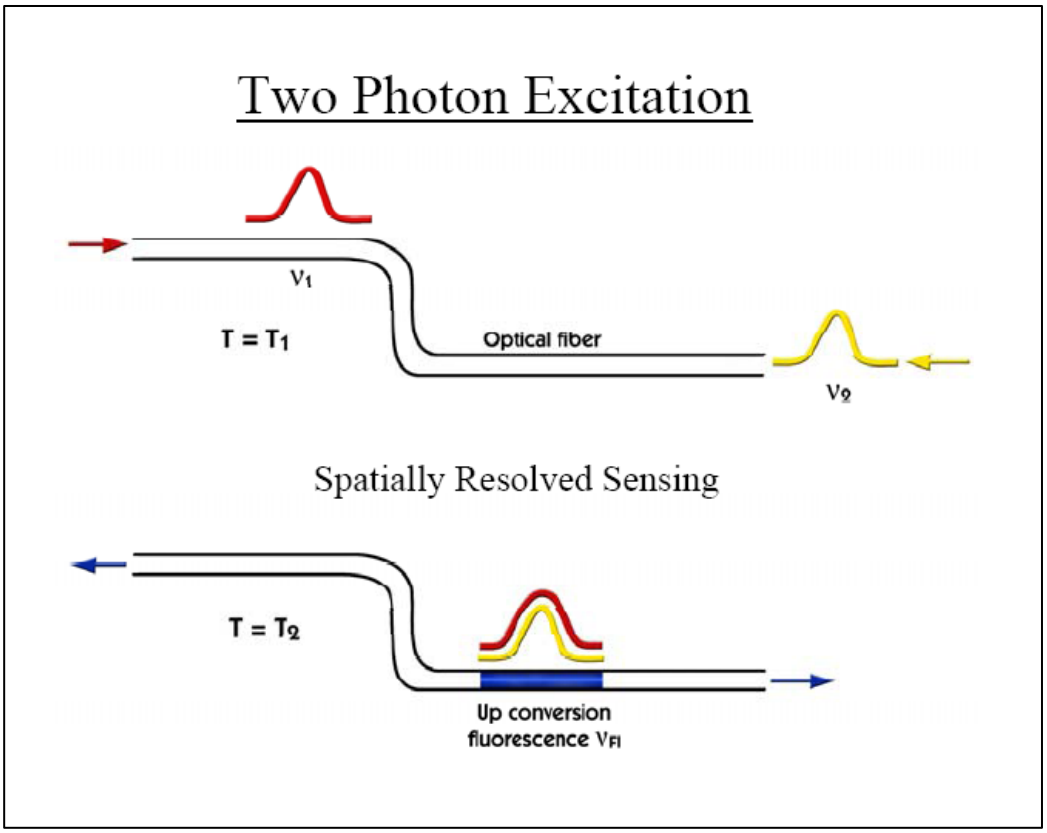

Figure 2-3: Two-photon distributed sensor scheme

By varying the timing of the excitation pulses, the exact position of the section of fiber being measured may be controlled. For this method to work properly, neither of the laser pulses would excite the fiber to the fluorescing energy state. Ideally, only when both pulses overlap would fluorescence be induced. For this situation to be able to occur, a suitable material would have to have an upper excited state from which spontaneous fluorescence would occur and lower excited states that do not fluoresce, at least not in the band of interest. A simple three state diagram illustrates this concept in Figure 2- 4. The spatial resolution of such a system may be set by a combination of

the length of the excitation pulse overlap and the decay time constant of the lower excited state.

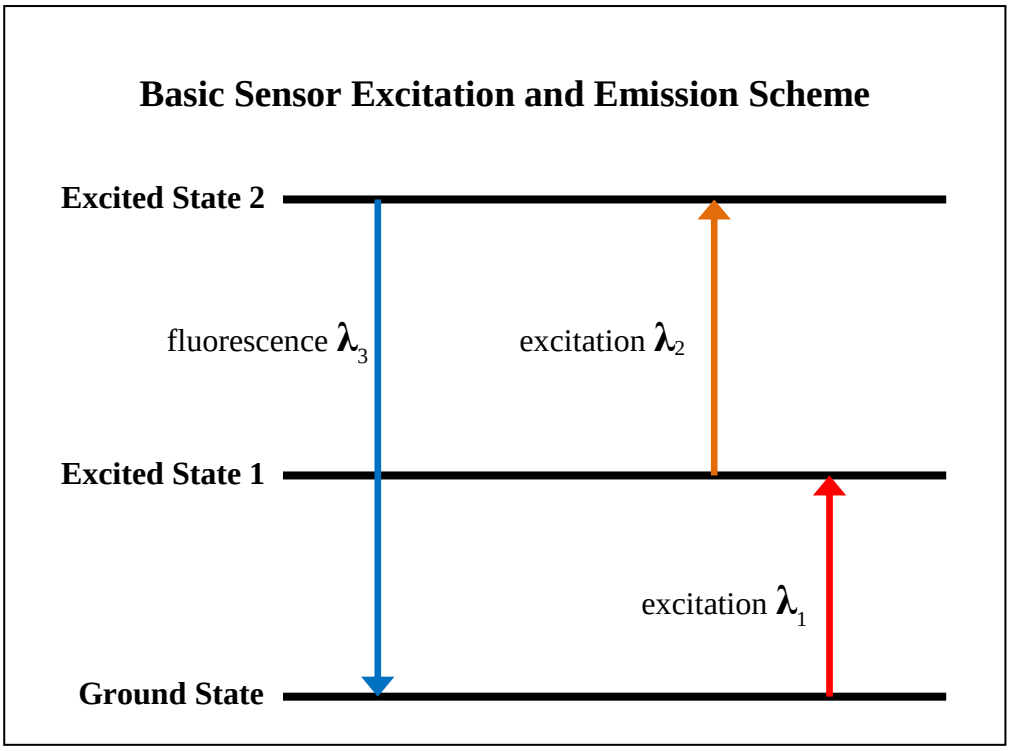

Figure 2-4: Simple energy band diagram for two-photon sensing scheme

Neodymium has an energy band structure similar to what is desired for this concept. The excited energy band structure of neodymium has been extensively studied in the past for use as a laser gain medium. The major difference between its use as a laser gain medium and the concept proposed here is that excitation process will be in two steps instead of one. Nd^{3+} is typically doped into a number of different host crystals and principally used as an ideal four-state laser gain medium as shown in Figure 2-5.

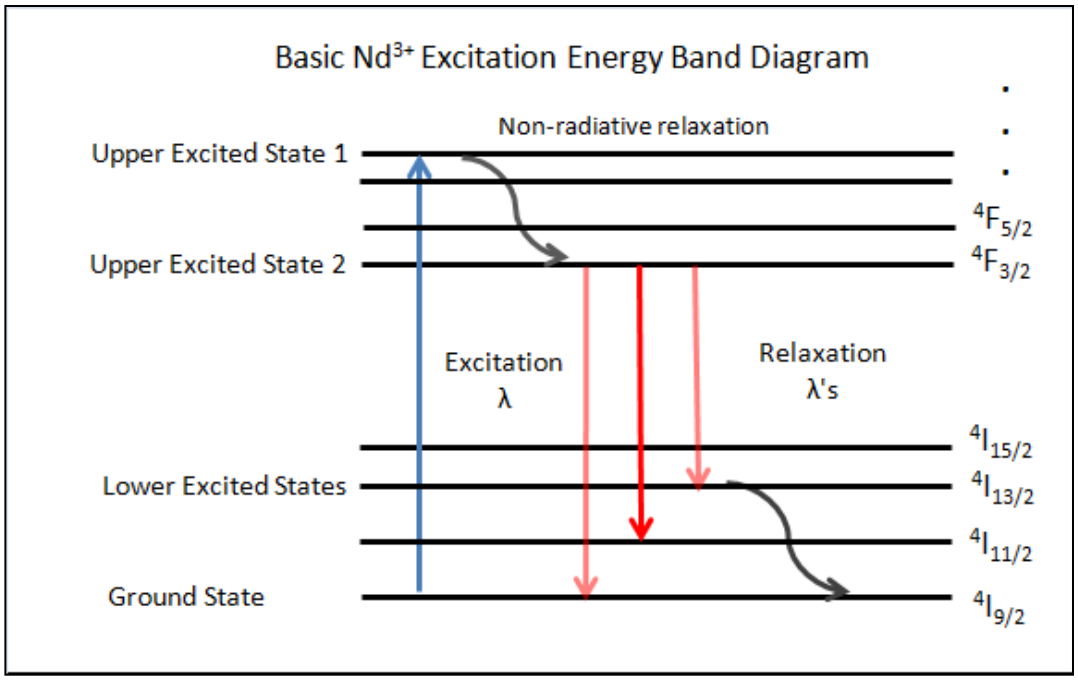

Figure 2-5: Nd3+ energy band diagram showing typical excitation process with key energy level assignments

As part of this thesis, I attempt to break up the excitation transition into a two-stage (two-photon) process. By exciting an electron into one of the lower excited states and then exciting it from there into one of the upper excited states, we can control spatially where the fiber is excited, and thus where the temperature is measured. A diagram of the proposed excitation process is shown in Figure 2-6.

To appropriately choose the excitation sources, the energies of the key Nd^{3+} in silica energy levels need to be determined. The spectroscopy of rare earth ions done by Dieke and Crosswhite[8] in 1963 as well as by Ainslie et al.[4] provides a good basis from which to begin the spectroscopy in this thesis. Their work helped to focus this investigation. Based on what they had found, this thesis focuses on the absorption

spectra of the upper states from about 400 nm to 1 um. In the lower energy states the $^4I_{15/2}$ energy level is the primary focus. The fluorescence emits in three bands ranging from approximately 800 nm to 1400 nm, depending on the host material. This thesis highlights some interesting behavior of neodymium fluorescence in a silica host.

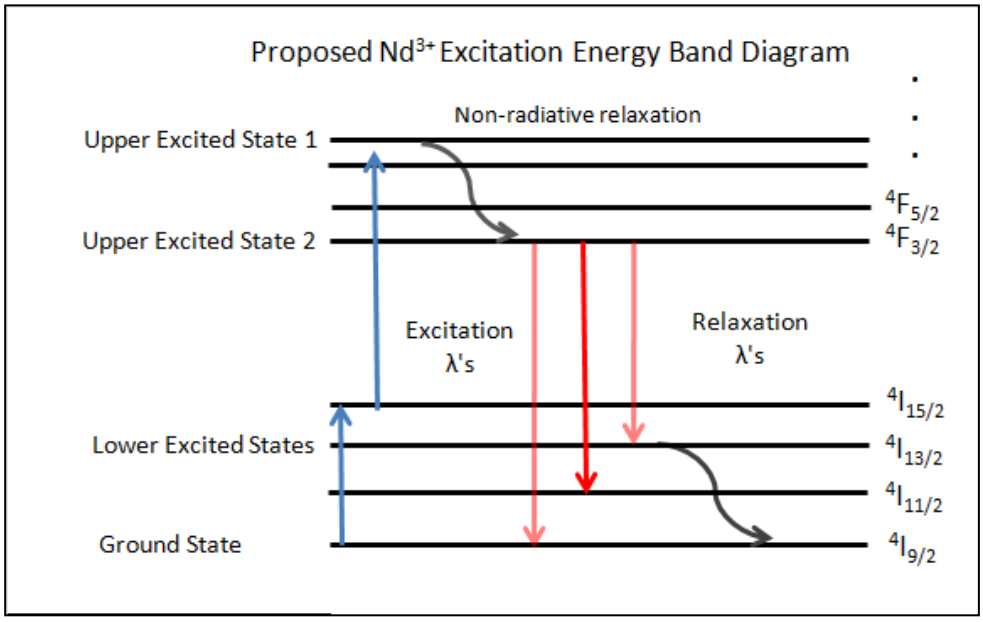

Figure 2-6: Nd3+ energy band diagram showing proposed excitation process with key energy level assignments

3 Nd^{3+} doped fiber spectroscopy

3.1 Introduction to Neodymium Spectroscopy

Why neodymium? Neodymium has been studied extensively. It is the second most plentiful rare-earth element, being not that rare. It is used in a number of different crystalline and non-crystalline hosts for use as laser gain media such as yttrium aluminum garnet (YAG), yttrium lithium fluoride (YLF), yttrium vanadate, and glass. This means that there has been a fair amount of spectroscopic research done with these materials. Some of this research is leveraged here to help investigate further Nd^{3+} doped materials for this application. Thanks to Oak Ridge National Labs, I also had access to two 10 meter lengths of Nufern Nd-doped double clad fiber.

One of the critical aspects of the proposed sensor scheme was to find practical excitation source lasers. Therefore it was important to characterize the absorption spectra of the Nd^{3+} samples. This enabled better selection of potential excitation lasers. In addition to matching laser sources to absorption peaks, the emission fluorescence was characterized for the purpose of signal detection and fluorescence decay time constant measurement.

3.2 Absorption Spectra

Based on the work done by, and using a method similar to, Ainslie et al.[4], a sample of a Nd^{3+} doped silica fiber was measured for its upper state absorption spectrum. The sample of fiber used was Nufern 27 μm irregular multimode core double clad fiber, intended for use as the gain media in a fiber laser. A picture of the

fiber cross-section is shown in Figure 3-1. Initially the doping concentration was unknown. From the absorption data collected in this thesis, and compared with data from Farries et al.[11] and Quoi et al.[20], it was determined that the sample of fiber that was measured had a doping concentration of approximately 0.03%. This sample of fiber was primarily used to characterize the upper energy states absorption spectra as well as to characterize the temperature dependent properties of neodymium in silica. An additional fiber sample with a higher doping concentration of 0.5%, and a core diameter of 9 μm, was used to obtain the absorption spectra for the lower $^4I_{15/2}$ energy level. Two additional neodymium host samples were measured along with the silica fibers for comparison: Nd:YAG and Nd:Glass (soda-lime).

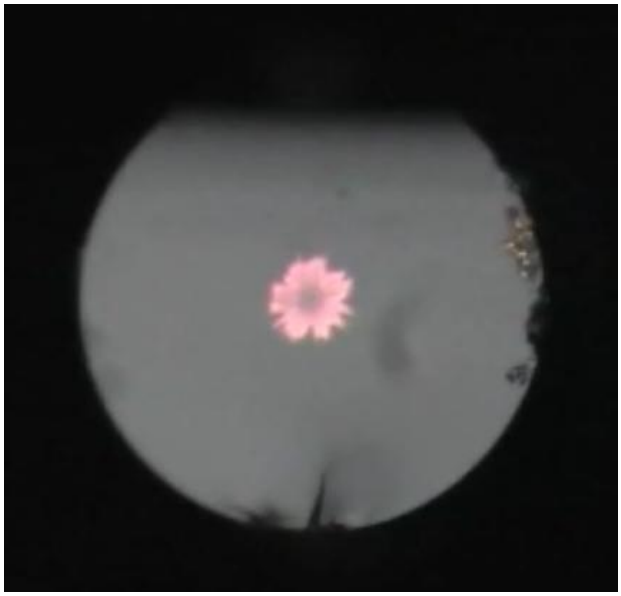

Figure 3-1: Cross-section of Nd-doped double clad fiber from Nufern

The absorption spectroscopy measurements were made primarily with one test apparatus configuration, with some variations in the specific equipment. The configuration that was used is diagrammed in Figure 3-2. Though one main configuration was used, several combinations of instruments and detectors were employed to cover the entire wavelength range that was measured.

The equipment used in the setup consisted of several components: a broadband light source, a monochromator, a lens system for matching the numerical aperture of the monochromator and the optical fiber, and some detection electronics, as well as the test sample being characterized. The broadband light source used to excite the fiber was a tungsten halogen lamp. This source output bandwidth was from about 400 nm to about 2500 nm according to the quartz transmission window. A 150 mm Acton monochromator was used with a 1 μm blazed grating used for frequency sweeping from 400 nm to 1 μm in the Nd samples. A ¼ meter Jarrel-Ash monochromator with a 2 μm blazed grating was used for frequency sweeping from 1 μm to 2.5 μm. A large area silicon photodiode was used for signal detection in the 400 nm to 1 μm band. In the case of the 1 μm to 2.5 μm band the high sensitivity of the photodiodes makes them a preferred choice for this sort of measurement but the narrow band sensitivity limits the bandwidth over which they can be used. Figure 3-3 shows the typical relative response range for several photodiode materials. None of these photodiode types would cover the needed range to measure the $^4I_{15/2}$ level so a Lead-Selenide photoconductor, whose spectral response band is between 1 μm to 5 μm, had to be used in this case.

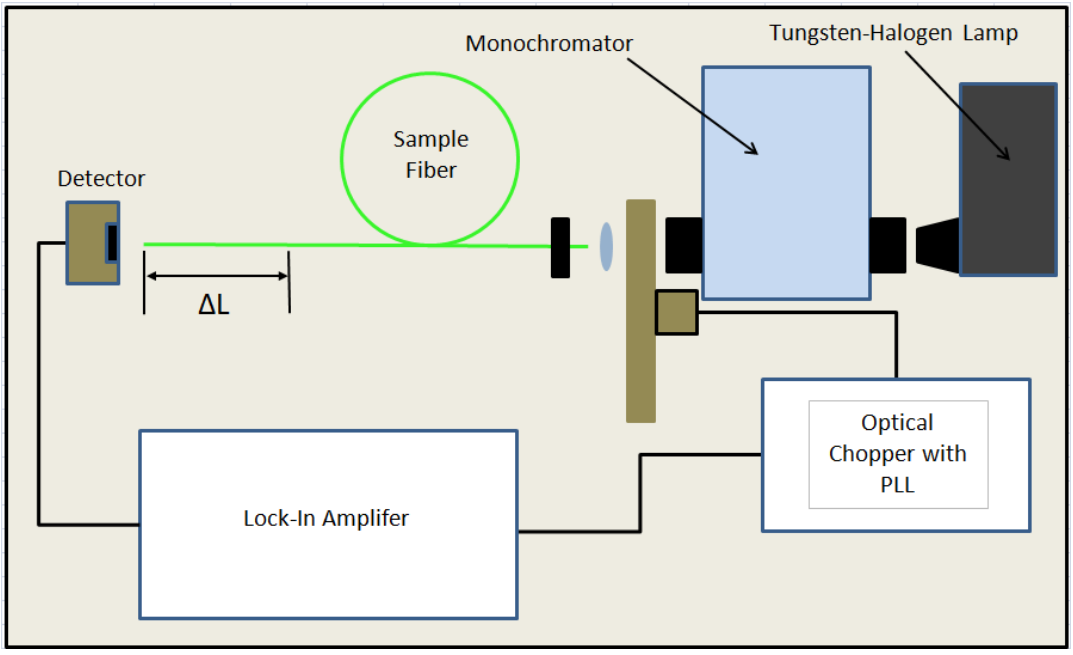

Figure 3-2: Experimental Setup for optical absorption spectra

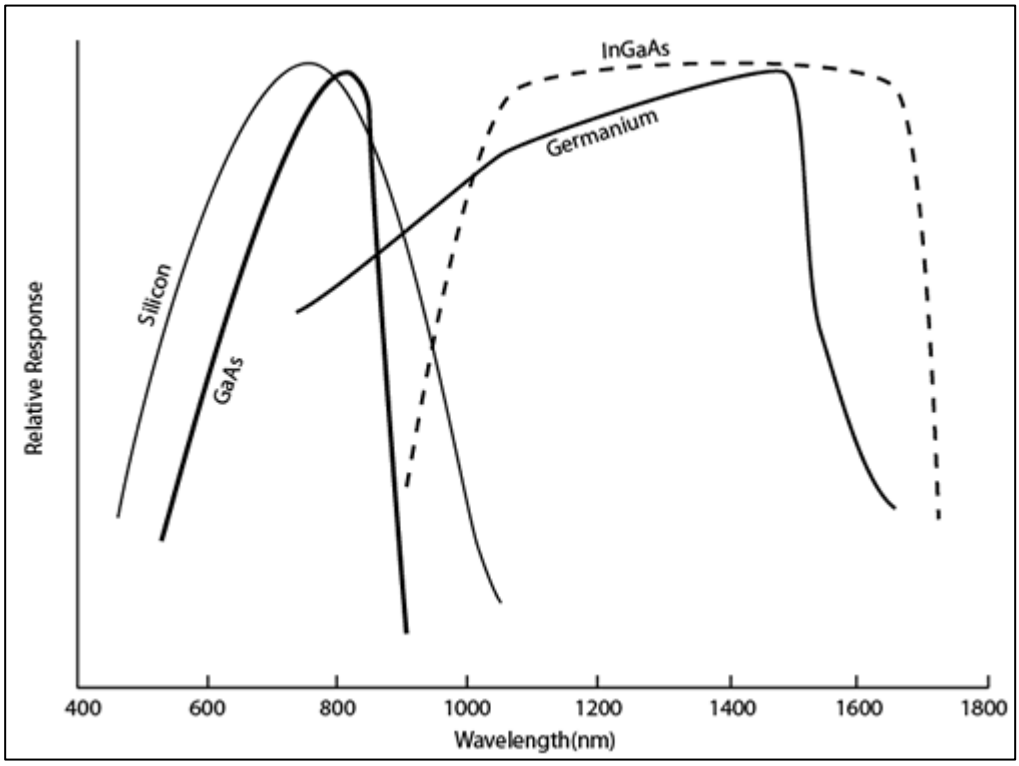

Figure 3-3: Relative detector response curves

The method used to measure the absorption magnitude for the 0.03% Nd optical fiber samples was the cut-back method. The cut-back method is a destructive test but it enables an accurate measure of absolute absorption magnitude. The cut-back method is employed by first preparing the fiber sample, which entails stripping back the buffer and applying index matching gel to strip out the cladding modes at the launch end of the fiber. All of the light from the output end of the fiber must impinge on the detector's active area for an accurate measurement. The sample is then scanned over the spectrum of interest.

After the initial scan, a known length of the fiber is removed from the output end being careful not to disturb the light coupling at the launch end of the fiber. Again, all of the light from the output end must impinge on the detector. Finally, a second scan is made on the sample. The absorption cross-section spectrum can then be determined and plotted by equation 3.1 where A is the absorption per unit length, S_1 is the scan of the longer length, S_2 is the scan of the shorter length, and L is the length of fiber removed.

$$\mathbf{A} = (\mathbf{10}\,\mathbf{log_{10}}\frac{\mathbf{S_2}}{\mathbf{S_1}})/\mathbf{L} \tag{3.1}$$

The cut-back method works well for optical measurements on optical fibers but does not necessarily work for optical measurement on other types of samples. For these other samples the substitution method is employed. The substitution method is much less satisfying when it comes to confidence in absolute absorption magnitudes.

Great care must also be taken in the optical setup so as to ensure quality of data. Specifically the output beam from the monochromator must be focused with a long enough focal length to ensure that the beam passes through the sample and impinges entirely on the detector active area with and without the sample in place over the wavelength range being tested. This required sample geometries that were appropriate for this test.

As was discussed previously, there were two distinct bands of the Nd^{3+} samples that were focused on in the absorption spectra. A resulting absorption spectrum of the upper band, which consists of energy levels that excite with near infrared through near ultra-violet, is shown in Figure 3-4. This particular spectrum was obtained by employing the cut-back method on a 120 cm long sample of neodymium doped fiber with a doping concentration estimated at 0.03%[16]. Even at this low doping concentration, the absorption between 575 nm and 600 nm is so strong that the transmitted light in that band becomes difficult to detect at fiber lengths much greater than the 120 cm length used to generate this curve. At this level of optical absorption the noise in the detector instrumentation becomes significant and makes it impossible to resolve the fine structure in that particular band.

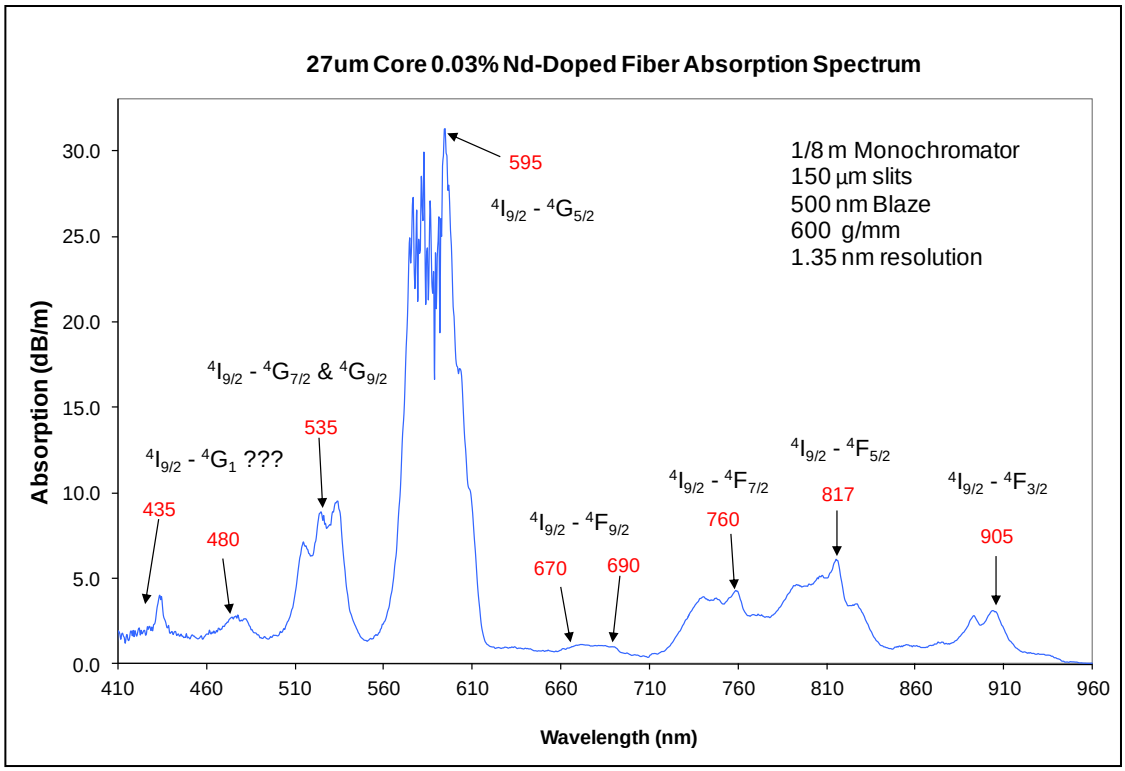

Figure 3-4: 0.03% Nd-doped fiber optical absorption spectrum for upper energy states

Since there is a tremendous amount of literature covering Nd:YAG spectroscopy, a Nd:YAG laser rod was also scanned alongside of the fiber samples for comparision. The purpose of this was to highlight the effects of the silica host on the Nd^{3+} energy level locations. Also, the aim was to identify the particular energy levels themselves based on the correlation of the peaks between the two curves. An additional spectrum of a Nd:Glass sample from a glass slab optical amplifier was also collected. This was done to contrast the effects of an additional host that was expected to be similar to the silica host in that it is amorphous, but similar to the YAG rod in the doping concentration. Figure 3-5 is a plot of the spectra of the three samples together.

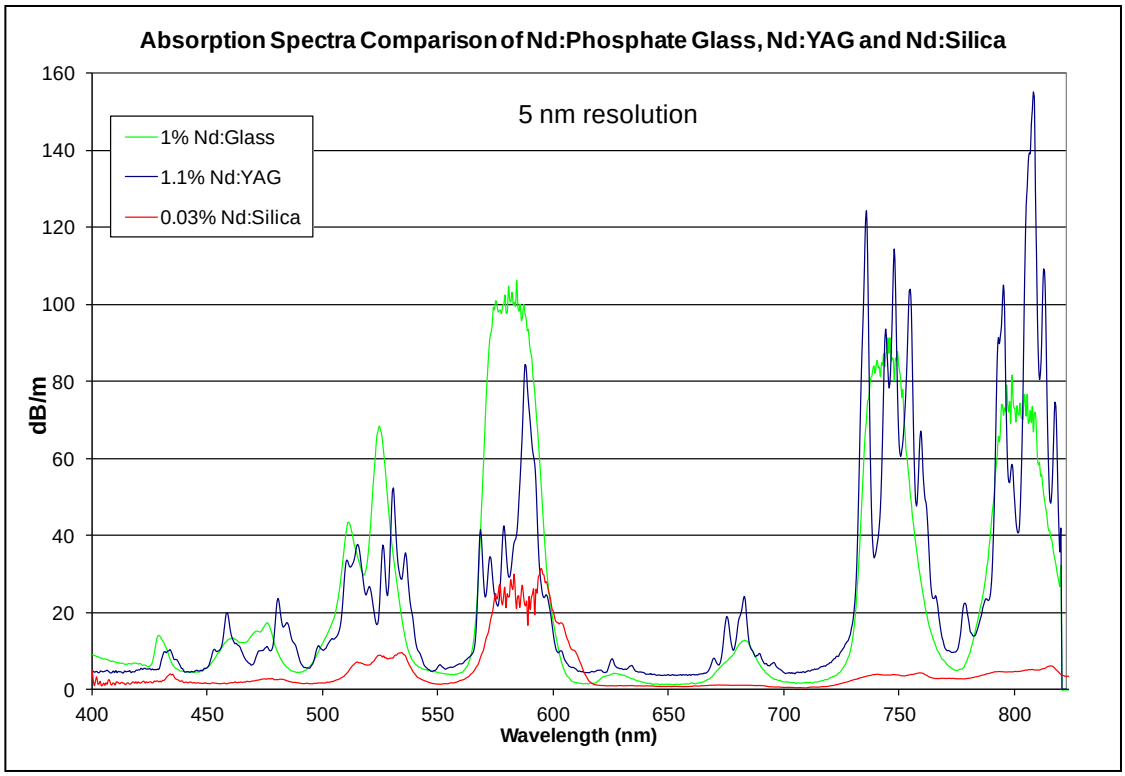

Figure 3-5: Optical Absorption Spectra for Nd:glass, Nd:YAG, and Nd:Silica

It is clear from this data that the main energy level bands are approximately in the same locations across the different hosts. However, the line broadening in the amorphous samples leads to a "smearing" of the energy level multiplets that are seen in the YAG host. There is also a shift in the relative magnitudes of the absorption peaks. It is quite evident that the peak absorption in the Nd:YAG is located at 808 nm whereas in the Nd:Silica fiber the peak absorption is located at 595 nm, and at approximately 580 nm in the phosphate glass host. From this data, transition assignments, shown in Figure 3-4, are given to the absorption bands in the Nd:Silica. These are based on the Nd:YAG energy levels given in Gruber et. al.[7] and Dieke and Crosswhite[8].

The $^4I_{15/2}$ energy level in Nd^{3+} was also investigated, since it is key to the proposed 2-photon scheme. This is the only energy level in the Nd^{3+} material that can be excited by readily available laser diode sources and does not cause fluorescence. This would likely need to be the level that is excited from the ground state for a linear 2-photon scheme to work. In Figure 3-6, the $^4I_{15/2}$ absorption spectra show that the 300 ppm Nd-doped fiber has a very weak absorption in that particular band.

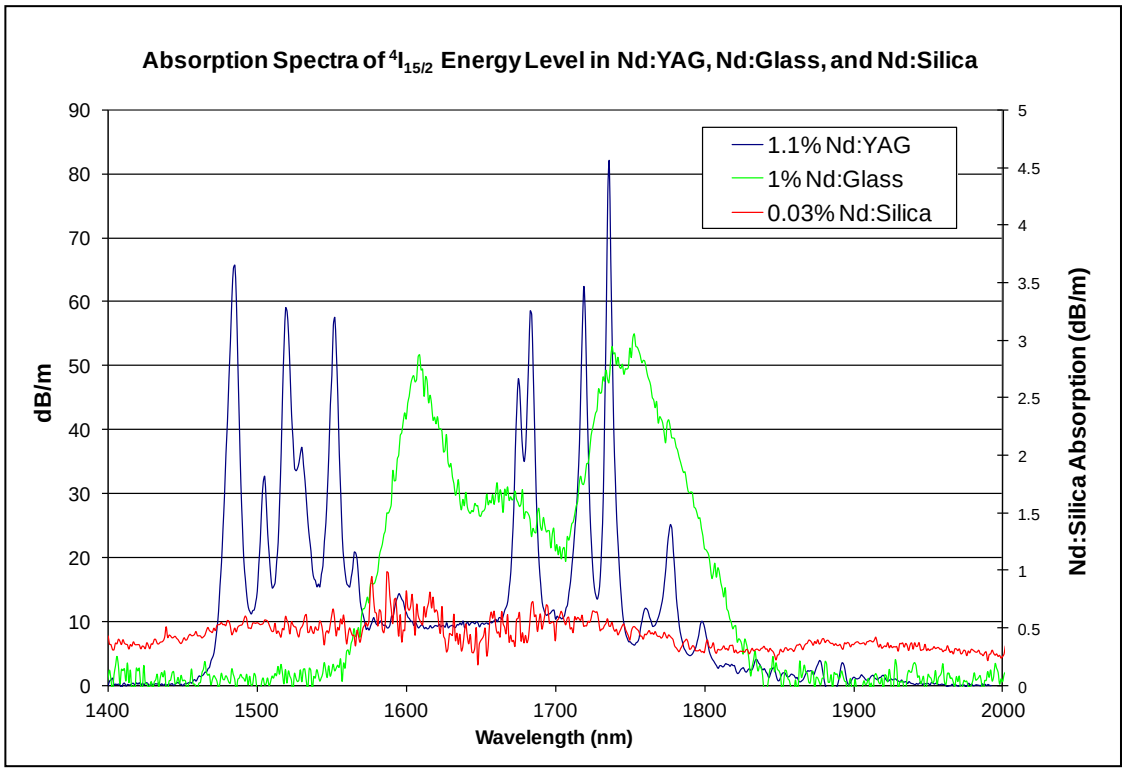

Figure 3-6: $^4I_{15/2}$ absorption band in Nd:silica (0.03% concentration), Nd:YAG, Nd:glass

The weak absorption led to the need for a more heavily doped sample to even get meaningful data. The 0.5% Nd:silica fiber was used for the spectrum shown in Figure

3-7. This particular sample was not measured using the cut-back method, so the data shown is only relative, but the increased neodymium concentration in the sample shows clear absorption peaks.

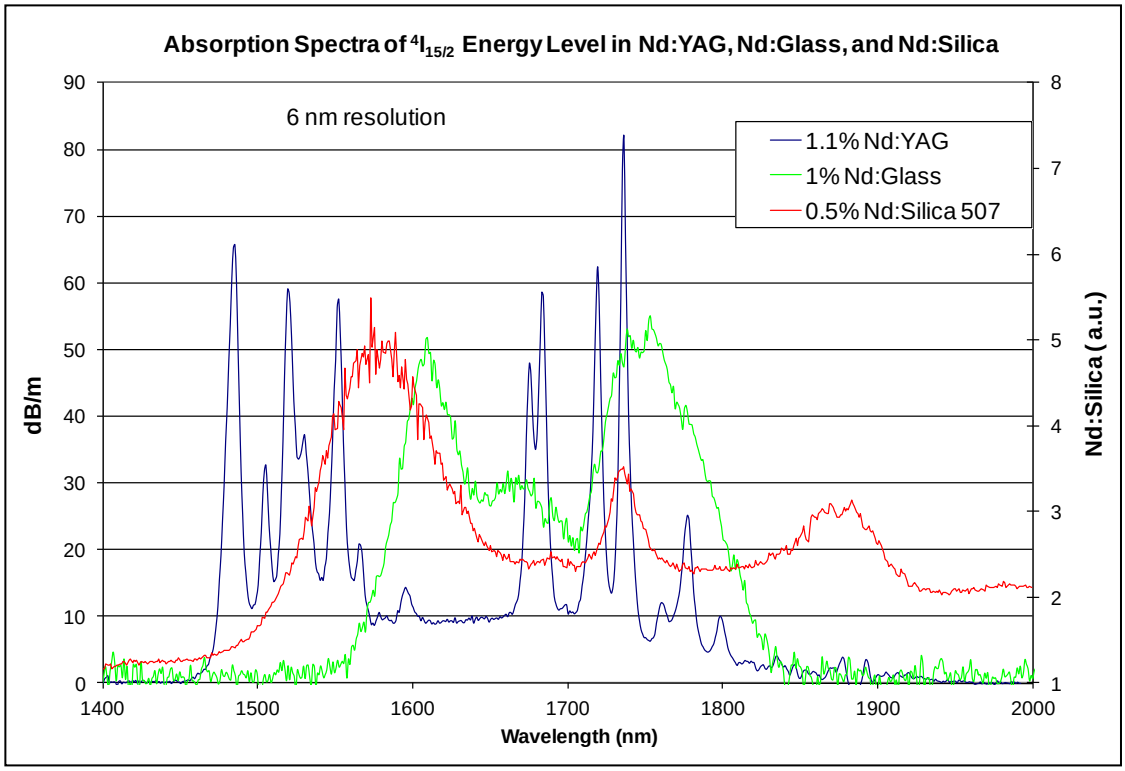

Figure 3-7: $^4I_{15/2}$ absorption band in Nd:silica (0.5% concentration), Nd:YAG, Nd:glass

The absorption band for the $^4I_{15/2}$ level in the three samples is broad. It is clear in Figure 3-7 that the peaks are shifted relative to each other. It is seen from the data that it may be possible to use a standard telecom diode laser to excite the peak which is located close to 1600 nm.

3.3 Fluorescence Spectra

In addition to the absorption spectra the emission spectra for three neodymium doped hosts is studied. It is well known that the primary radiative transition in Nd:YAG is from the bottom of the upper states ($^4F_{3/2}$) to three of the four lower energy states [9]. Due to the strong absorption band measured at 532 nm shown in figure 3-3, a doubled Nd:YAG laser was used to excite the $^4G_{7/2}$ level, which then non-radiatively decays down to the $^4F_{3/2}$ metastable level. This level then experiences relaxation down to the four lower levels, which in turn non-radiatively decay to the ground state. It was the fluorescence from the radiative transitions from the $^4F_{3/2}$ to the three lower levels ($^4I_{9/2}$, $^4I_{11/2}$, $^4I_{13/2}$) in the Nd:silica fiber that was measured using the apparatus shown in Figure 3-8.

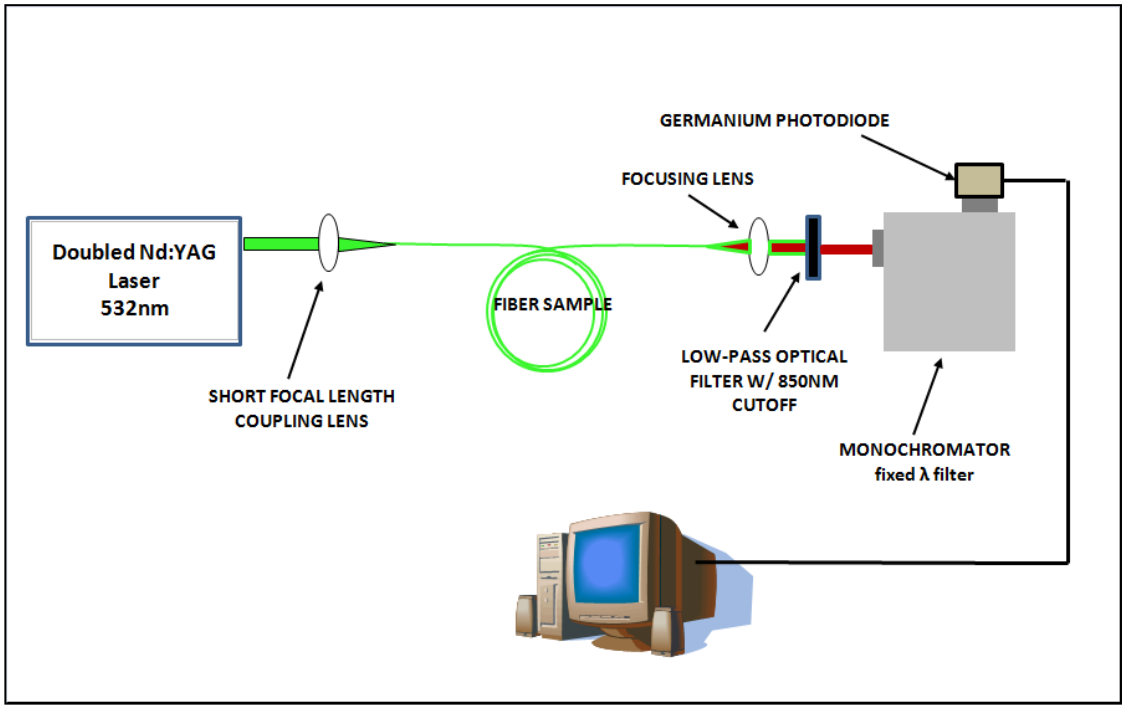

Figure 3-8: Experimental setup for Nd-doped optical fiber fluorescence spectroscopy

For a neodymium doped silica host the data collected in these experiments show that the excited emission falls into three bands: the first band is from ~900-980 nm, the second from 1020-1190 nm, and the third from 1340-1490 nm. These emission bands can be seen in Figure 3-9. It is understood that the three bands correspond to the energy level transitions; $^4I_{9/2}$-$^4F_{3/2}$, $^4I_{11/2}$-$^4F_{3/2}$, and $^4I_{13/2}$-$^4F_{3/2}$. Emission to the $^4I_{15/2}$ level was not detected. If it were present it would likely fall around the 2 μm wavelength. This result appears to be confirmed by Liao et. al.[15] who indicates that this is a multi-phonon process instead. Additionally, these measurements were made on glass and YAG hosts as well and the data is presented in Figure 3-10 as a composite for comparison.

This data also shows that all three of the emission bands seem to come from relaxation of one common upper energy state down to three of the four lower level states. This was confirmed in this research by exciting a number of the absorption bands shown in Figure 3-4. When neodymium is excited into one of its upper level energy states, it will non-radiatively relax down to the lowest of the upper level energy states ($^4F_{3/2}$), and then radiatively relax down to one of the lower level states.

The relative magnitudes of the emission shown in this data do not take into account the spectral efficiencies of the monochromator or germanium detector. However, neither efficiency curve is steep in the area of interest so the relative magnitude of the emission in Figure 3-9 and 3-10 can be viewed qualitatively.

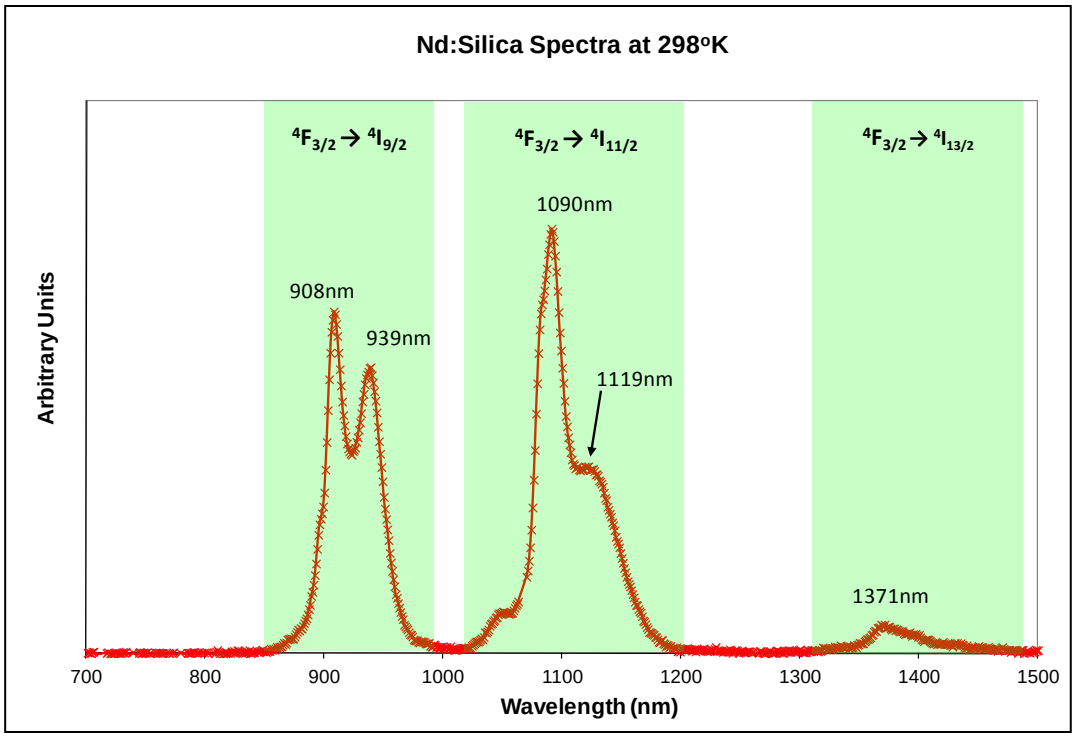

Figure 3-9: Nd:Silica fluorescence bands

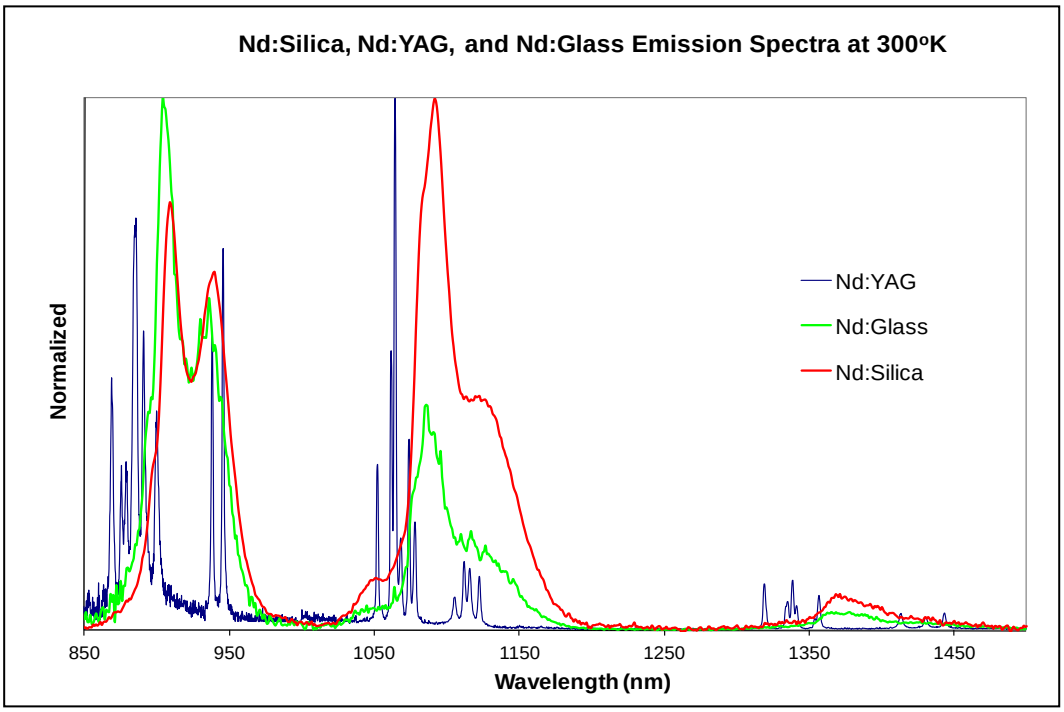

Figure 3-10: Fluorescence spectra of Nd:Silica, Nd:YAG, and Nd:glass

According to the Nd energy level diagram in Figure 2-5 it seems that the emission to the $I_{9/2}$ would appear to be to the ground state. But upon further examination and testing, by stripping the cladding modes, we are able see that the emission peak at 908nm drops. This indicates that the light traveling in the doped core of the fiber is partially reabsorbed. This means that it does indeed appear to be relaxation to the ground state and will indeed be re-absorbed/emitted (Figure 3-11). The neighboring peak however, at 940nm, does not appear to be emission directly to the ground state. So it does not appear that the multi-peak nature of the emission is due to level splitting in the $^4F_{3/2}$ energy upper energy but rather it is due to level splitting in the lower energy band.

Therefore it seems that the spectral structure of the neodymium fluorescence is given not by the upper state energy level but by the lower energy states. It follows that since all of the emission relaxes from a single upper state the structure of the lower three energy levels can be inferred from the spectral structure of the emission. This energy band structure is especially evident in the Nd:YAG sample in Figure 3-10. Calculations of the energy level locations from this data were later used to select excitation sources to test the 2-photon excitation scheme.

In the case of this first emission band centered about 920nm it appears that the lower energy band at $^4I_{9/2}$ is split and not fully populated. The Boltzman energy level is calculated to be 207 cm^{-1} for 25 °C and 259 cm^{-1} for 100 °C. Since the gap between the 908 nm and 940 nm peaks is equal to 375 cm^{-1} it follows that over the proposed temperature range of the experiments in this thesis we would not expect for the upper

portion of the $^4I_{9/2}$ level to be thermally populated. So the 940 nm emission should not stimulate this material from the ground state. This means that the 940 nm peak is a candidate for the multi-photon excitation process while the 908 nm peak is not.

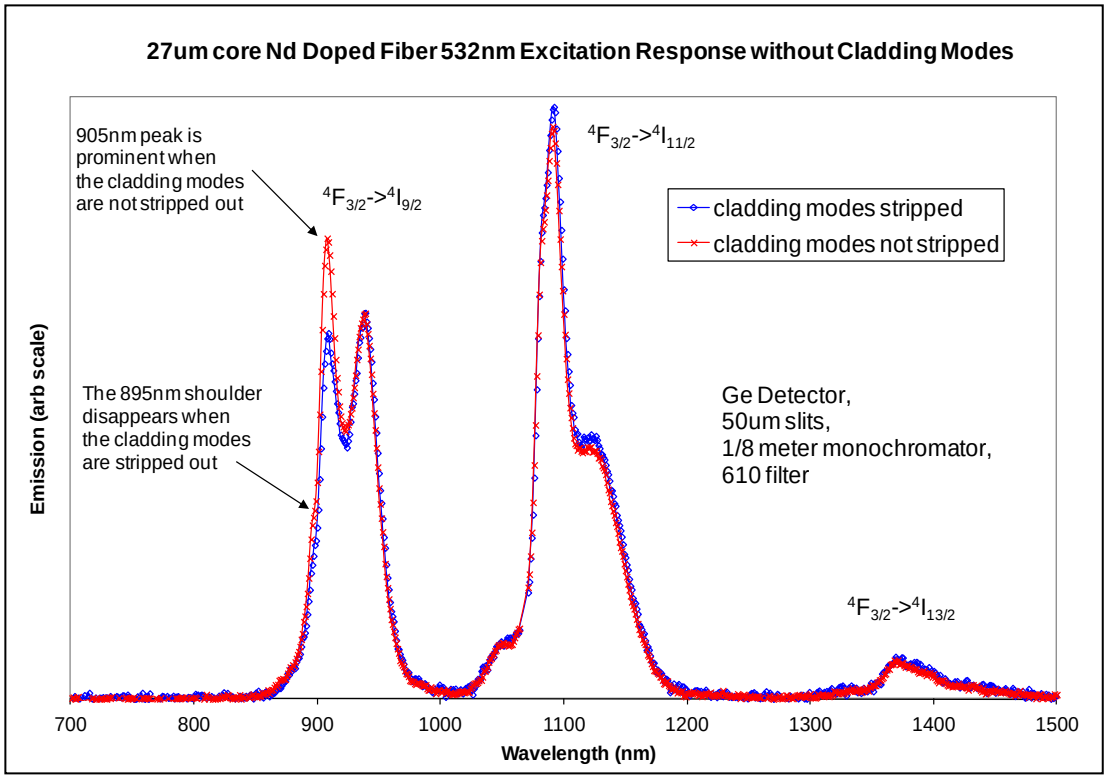

Figure 3-11: Nd:Silica fluorescence in optical with and without cladding modes

4 Fluorescence Temperature Dependent Behavior

As it was discussed in chapter 2, rare-earth doped phosphors have been demonstrated to have temperature dependent fluorescence lifetimes, even using this behavior in devices employed in extreme applications. Similarly, Grattan et. al.[14] characterized the temperature dependent nature of the fluorescent lifetime for the $^4F_{3/2} \rightarrow {}^4I_{11/2}$ relaxation in Nd:YAG for the 1.064 μm line, shown in Figure 4-1. In this chapter, the temperature dependent fluorescence of Nd:silica is characterized. Specifically, this research focuses on the two principle fluorescence peaks at 908 nm and 940 nm for the $^4F_{3/2} \rightarrow {}^4I_{9/2}$ transition and the peak at 1090 nm for the $^4F_{3/2} \rightarrow {}^4I_{11/2}$ relaxation. Additionally, the fluorescence amplitude vs. temperature is also characterized for the ground state relaxation.

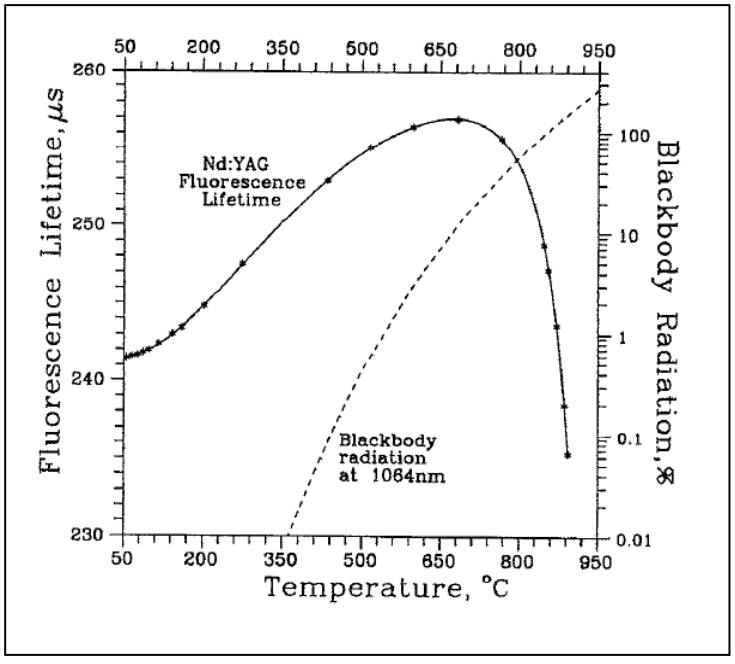

Figure 4-1: Temperature dependent fluorescence lifetime in Nd:YAG (1.064 μm)

4.1 Experimental Setup

A sample of 10 meter long 27 μm neodymium doped silica fiber, with a doping concentration of about 300 parts per million, was tested for its temperature dependent fluorescence time decay behavior. The fiber was heated in an aluminum block (oven) using a resistive heating element. The temperature was varied manually by adjusting the voltage on the element. The temperature of the block was monitored using a K-type thermocouple. At various temperatures, the fiber was excited by a pulse train from a 532 nm doubled Nd-YAG Q-switched laser. The fiber fluorescence was focused into a 1/8 meter Monochromator with a 600 g/mm grating and 1mm slits, giving a resolution of 9 nm. The Monochromator was used to select specific bands of emission for investigation. Additionally, an 800 nm low-pass step bandpass optical filter was used to block residual excitation light. For each excitation pulse, the signal from the fiber was measured using an avalanche photodiode (APD) and a TDS220 oscilloscope. The trace from each pulse is sent to a computer and many pulses are averaged to determine the time constant. The experimental setup is very similar to that shown in Figure 3-8 except that the fiber is now thermally perturbed and the signal collected is time based. A picture of the apparatus is shown in Figure 4-2.

When the neodymium fiber is excited with a short pulse from the laser the fluorescence pulse looks like that shown in Figure 4-3. If the excitation pulse is sufficiently fast, in comparison to the fluorescence lifetime, it does not need to be accounted for in the decay time measurement. Specifically, the falling edge of the pump pulse must be fast enough to not be convolved in the decay of the fluorescence.

In this case the excitation pulse was a Q-switched 40 ns long pulse with a falling edge on the order of 10 ns long. This excitation profile acts essentially like a delta function in comparison to the several hundred microsecond long decay time of the neodymium sample.

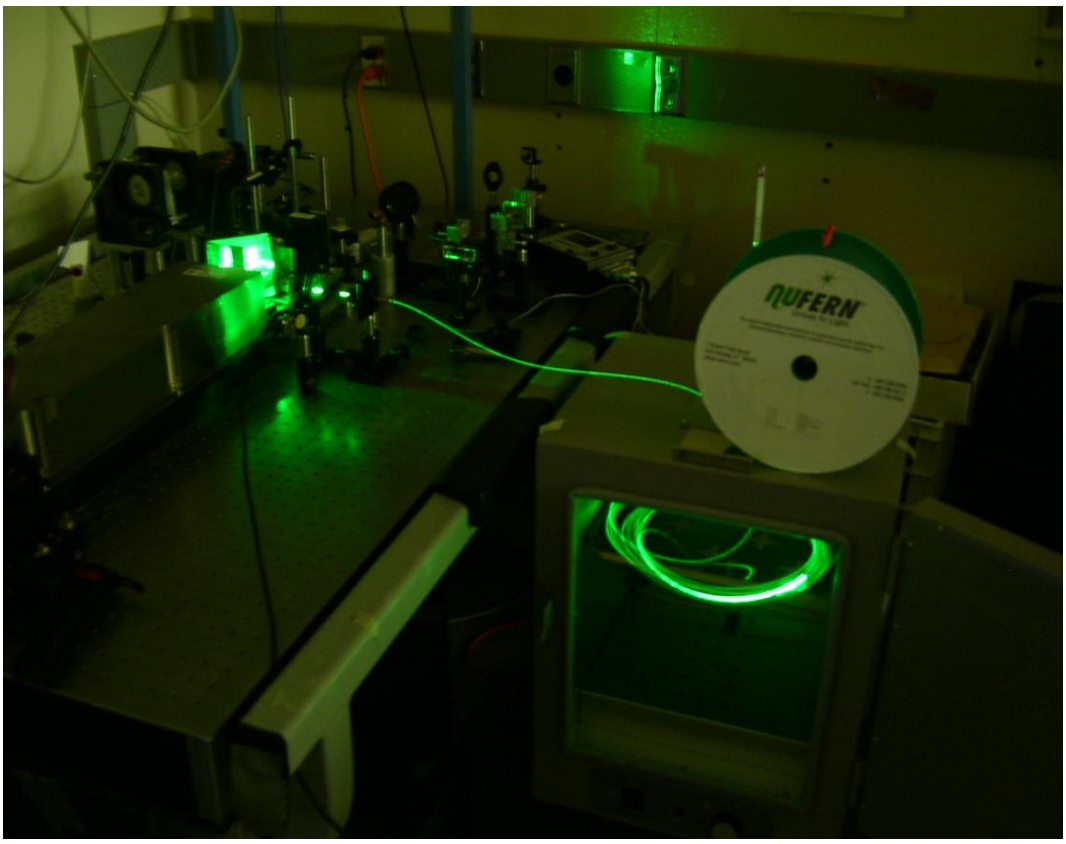

Figure 4-2: Picture of fiber sample being optically excited in oven

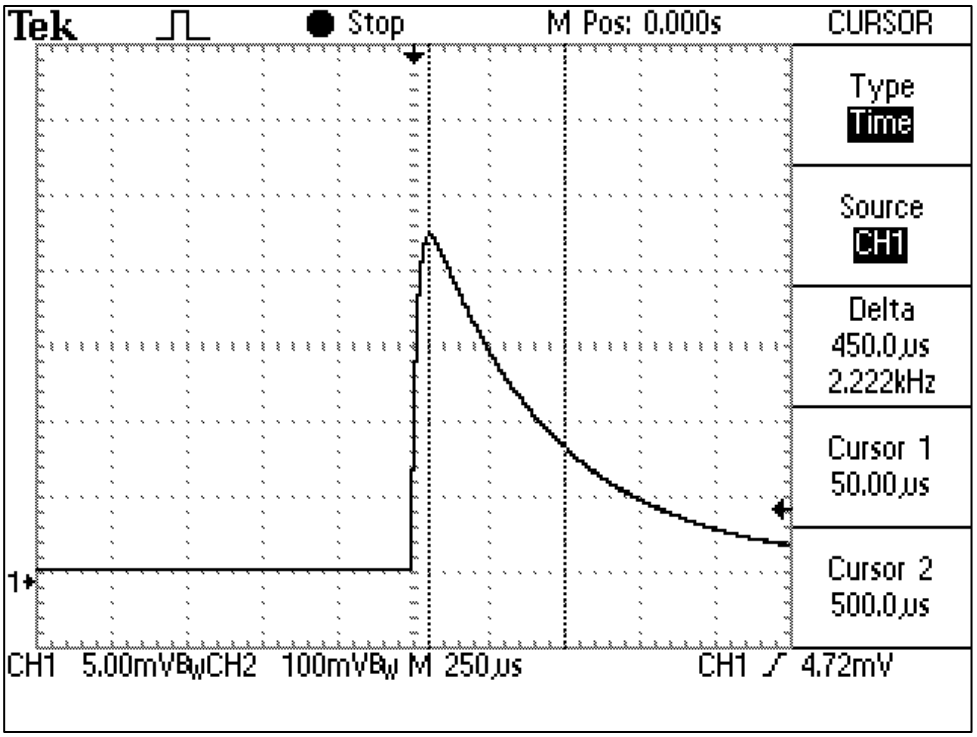

Figure 4-3: Fluorescence decay from pulsed excitation in Nd-doped optical fiber

The generalized time domain decay response of the neodymium fiber, when excited with a pulse that is much shorter than the longest fluorescence decay time constant, is given by the following equation;

$$A(t) = \sum_{n=0}^{n} A_n e^{\frac{-t}{\tau_n}} \tag{4-1}$$

A(t) is the relative fluorescence amplitude of the sum of different radiative decays at time t. τ_n is the 1/e time decay constant of each radiative component. If the fluorescence is filtered to select only one spectral component then it can be assumed that there is only one dominant exponential decay time constant present. This makes it

possible to quickly determine the time constant of a given pulse by taking the natural log of the previous expression.

$$\ln A(t) = \ln A + \frac{-t}{\tau} \tag{4-2}$$

If the data set is normalized in advance, it simplifies equation 4-2 further to equation 4-3 where we can see that the slope of the new expression is **-1/τ.** This is a quick way to determine the decay time constant of a pulse from a data array.

$$\ln A(t) = \frac{-t}{\tau} \tag{4-3}$$

4.2 Results

The emission peaks at 908 nm and 940 nm corresponding to the $^4F_{3/2} \rightarrow {}^4I_{9/2}$ transition and the 1090 nm corresponding to the $^4F_{3/2} \rightarrow {}^4I_{11/2}$ transition were investigated. The results for these measurements are shown in figures 4-4 thru 4-6. The data shows that the emission peaks at 908 and 940 nm exhibit similar results with both temperature coefficients and with decay time. While the peak at 1090 nm shows distinctly different behavior. Whereas the 908 and 940 nm peaks are measured with a temperature coefficient of ~ -0.3 μs/°C and a measured room temperature decay time of 481 μs and 425 μs respectively. The peak at 1090 nm has a positive temperature coefficient at 0.46 μs/°C with a room temperature decay time constant of 520 μs.

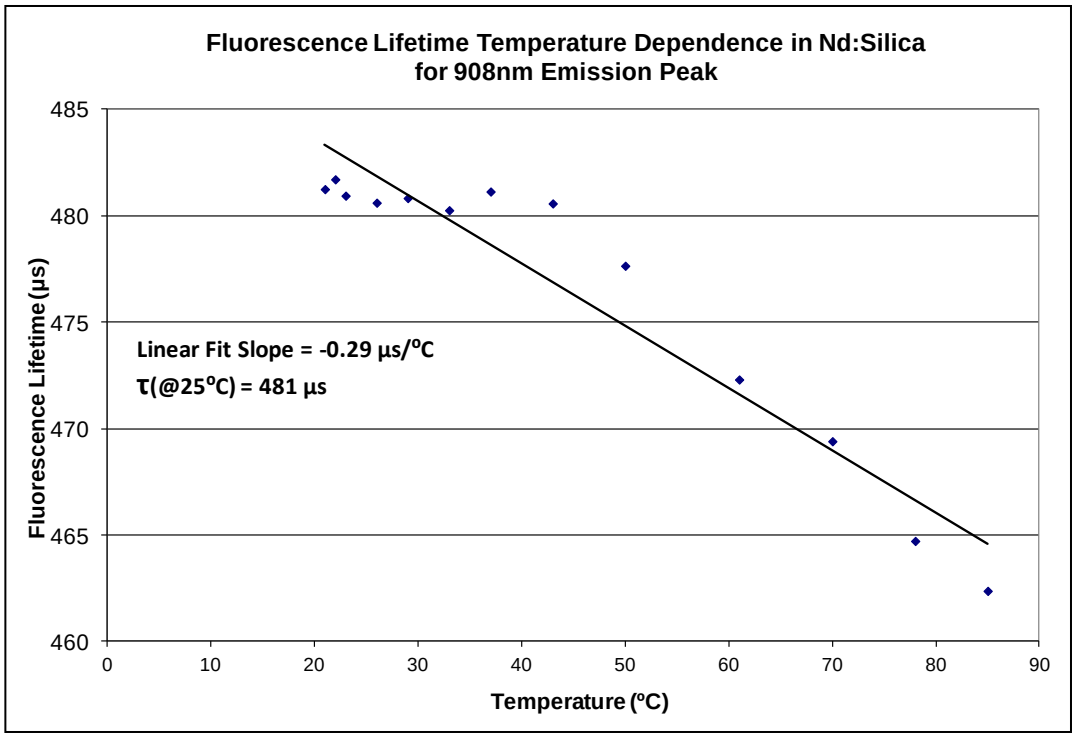

Figure 4-4: Temperature dependent fluorescence decay time constant for 908 nm emission

The behavior of the ${}^4F_{3/2} \rightarrow {}^4I_{11/2}$ emission shown in Figure 4-6 is consistent with the measured behavior of the 1.064 µm emission in Nd:YAG by Grattan et al.[14]. The long fluorescent lifetimes show that the doping concentration is relatively weak and so ion interaction should not be a significant effect. It is not clear what mechanism is causing the positive temperature coefficient at lower temperatures but the body of literature does indicate this behavior is actually nonmonotonic and that at higher temperatures the temperature coefficient will reverse direction and go strongly negative.

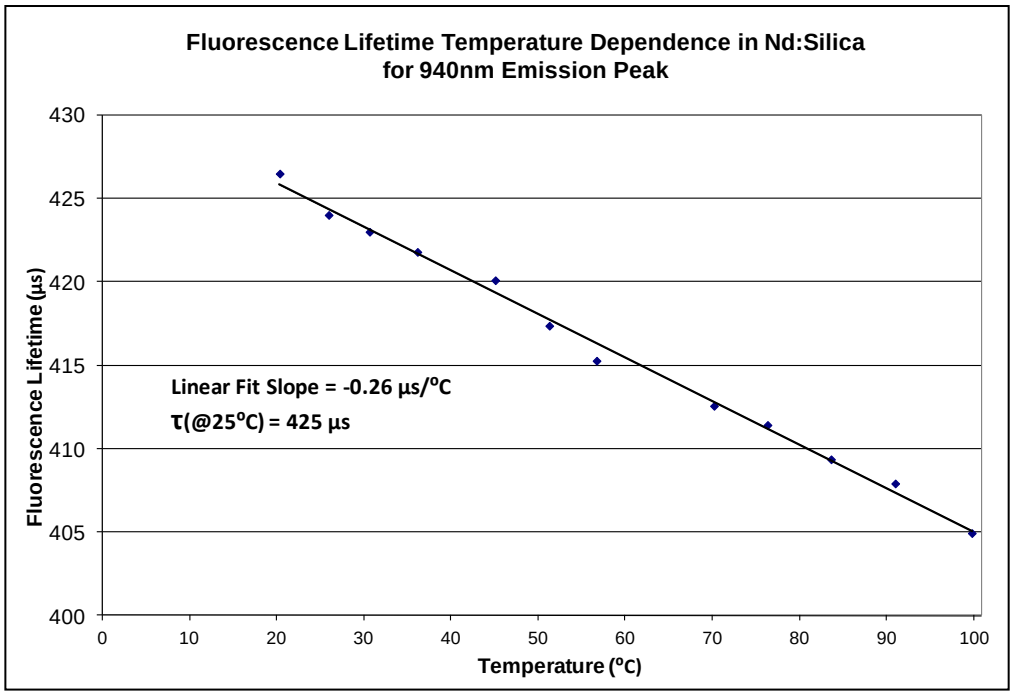

Figure 4-5: Temperature dependent fluorescence decay time constant for 940 nm emission

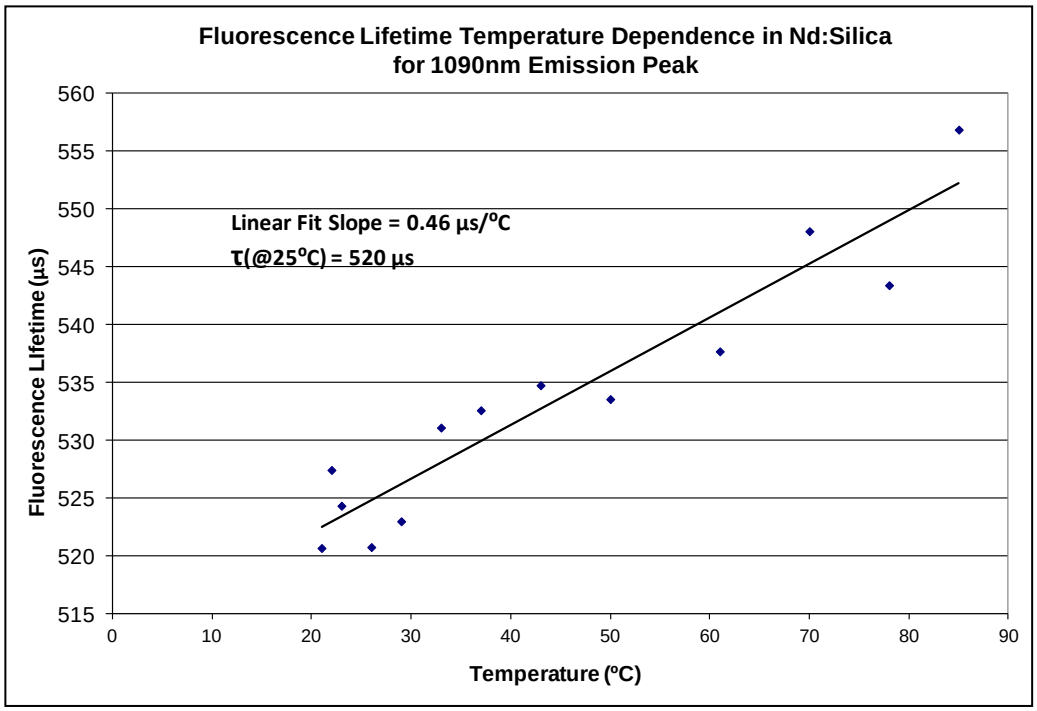

Figure 4-6: Temperature dependent fluorescence decay time constant for 1090 nm emission

One other interesting effect was noted while characterizing the thermographic behavior of the Nd optical fiber. The amplitude of the spontaneous emission was measured to decrease linearly with temperature increase. This effect is shown in Figure 4-7. In a laser, this effect would be characterized as thermal quenching [3] and is caused by multi-phonon relaxation from the excited meta-stable state down to the ground state. In a laser this would be a cause of lower efficiencies and higher lasing thresholds and would be characterized as negative property. But it appears to be the reason that the fluorescence lifetime responds linearly to temperature. This effect is a net positive for thermographic sensing using Nd:silica fiber. The quenching behavior shown in Figure 4-7 does seem to confirm the assumed underlying multi-phonon relaxation as the driving mechanism for the linear and negative going temperature coefficient for the $^4F_{3/2} \rightarrow {}^4I_{9/2}$ transition.

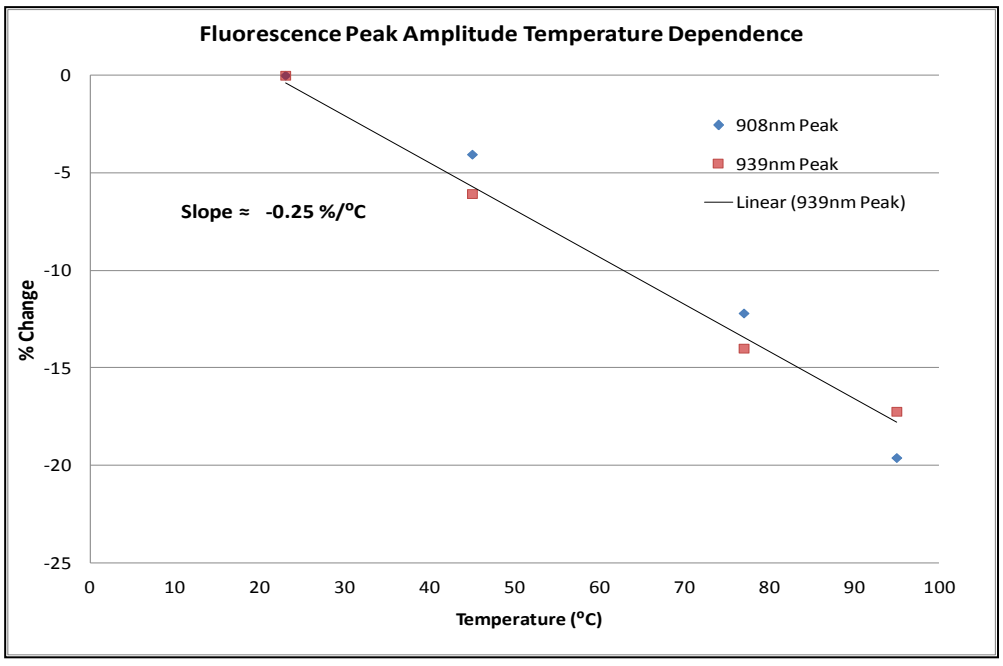

Figure 4-7: Temperature dependence of fluorescence amplitude

The 1371 nm peak in the $^4F_{3/2} \rightarrow {}^4I_{13/2}$ transition was not investigated. This was mainly due the small branching ratio for this transition, equating to a small detectable signal, and the availability of a suitable detector. As it was described earlier most of these measurements were made using a silicon avalanche photodiode (APD) whose bandgap energy is 1.1 eV. This equates to a photon wavelength of approximately 1.1 μm. This means that the Si APD can't be used to measure the 1371 nm fluorescence peak. Usually germanium or InGaAs photodiodes are used for wavelengths ranging between 1 μm to 1.7 μm. Germanium photodiodes are particularly noisy and not suitable for small signal measurements such as these. The InGaAs APD does have better noise characteristics when compared to germanium and would be the detector choice in this case. The measurement will still have signal amplitude challenges. First, the apparent branching ratio between the $^4F_{3/2}$ - $^4I_{9/2}$ and the $^4F_{3/2}$ - $^4I_{13/2}$ appears to be close to 10 to 1. Combine this with the difference in quantum efficiencies between silicon and InGaAs which comes out to be about 25% lower for InGaAs, as shown in Figure 4-8. The quantum efficiency curves in Figure 4-8 are typical but do vary for particular device designs. This particular graphic can be found at the following URL: http://www.fiberoptics4sale.com/wordpress/pin-photodetector-characteristics-for-optical-fiber-communication/. I also marked this graphic showing where the 908 nm emission peak lines up versus the 1371 nm peak. The emission from the $^4F_{3/2}$ - $^4I_{9/2}$ transition is optimally situated for detection by a silicon based detector. In contrast the emission from the $^4F_{3/2}$ - $^4I_{13/2}$ transition will require a more expensive indium gallium arsenide or germanium pin photodiode for detection.

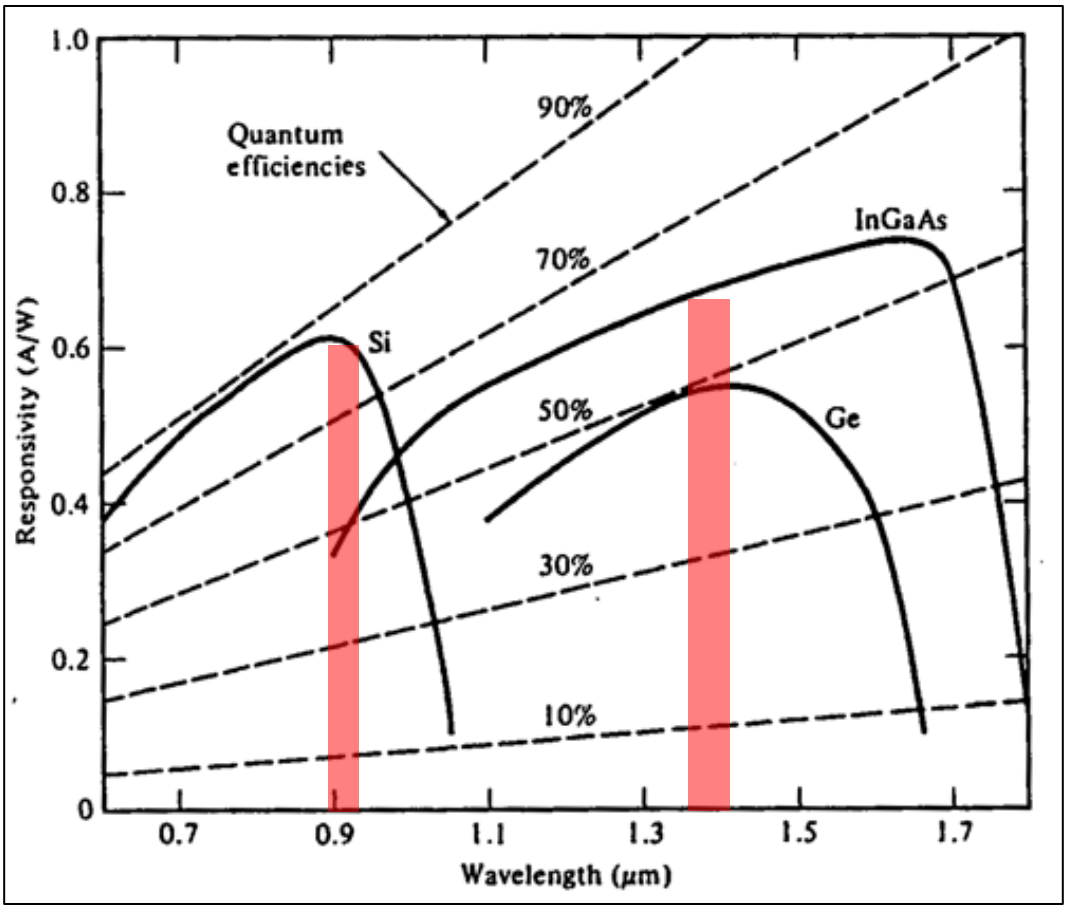

Figure 4-8: Quantum efficiencies of different semiconductors

Finally, an InGaAs APD has a much lower reverse breakdown voltage than a Si APD. Larger reverse voltages translate to gain in an APD. Typical maximum gain for an InGaAs is 20 which is much lower than for a Si APD which can range between 100 to 1000 depending on the breakdown voltage that can be applied. If all of this is taken together it can be expected that the measured signal from the 1370 nm emission peak will be between 50 to 100 times smaller than that made on the emission peak at 908 nm. This makes it much less likely to be a practical measurement in a DTS sensor design.

5 Two-Photon Upconversion from Lower Excited States of Nd-doped hosts

Key to the idea of the sensor proposed in this thesis is the notion of a two-stage excitation, or a two-photon upconversion. As stated previously in chapter 2, this would require excitation up to the lower excited states and then up to one of the upper excited states in a two-step process. Once excited into one of the upper excited states there would be phonon relaxation down to the meta-stable $^4F_{3/2}$ state.

Unfortunately, two-photon upconversion was not achieved in this study using the lower excited states in Nd-doped materials. The rest of this chapter will cover the experiments made, the reasoning behind them, and why it may have been that two-photon upconversion was not observed.

For this experiment it was important to select the appropriate sources so that the detected emission from the sample was from a two step process and not a single step ground state excitation. Based on the absorption and emission data taken previously, it was determined that any stimulating signal with a wavelength shorter than approximately 910 nm (11000 cm^{-1}) would cause ground state absorption to the upper excited states effectively eliminating the ability to spatially interrogate the fiber. Additionally, the energies of the lower excited states posed a problem for finding practical excitation sources. Since this device is focused around using a fused silica fiber, the optical transmission window also sets a lower energy floor for the possible excitation sources. The strong $^-$OH absorption in fused silica starts at approximately

2500 nm (4000 cm^{-1}). Therefore sources were chosen between the energies of 11000 cm^{-1} and 4000 cm^{-1}.

Initially a Ti:Sapphire OPA was used to generate the lower excitation signal. Since this source is tunable it could be used to scan through the energy band shown in Figure 5-1. The transitions assigned in this figure are based on the work by Guber[7]. Due to the nature of this type of laser the excitation pulses have very short (~100 fs) pulse lengths. This short pulse length causes a very high peak power and easily created detrimental nonlinear effects when concentrated in the core of the optical fiber. For this reason it was not possible to use the optical fiber with this source. Instead, a Nd:YAG rod was used as the test sample when this source was used.

In addition to the Ti:Sapphire source, two other lasers were used separately to provided one of the excitation steps, a 10 watt Q-switched Nd:YAG (1064nm) and a 10 watt CW Yb-doped fiber laser (1112nm). Table 5-1 lists the pumping schemes that were employed using the Ti:Sapphire source. These sources were aligned such that the two pump beams ran orthogonally to each other, as well as to the Silicon APD used as the signal detector, and crossed within the sample material at a single point as shown in Figure 5-2.

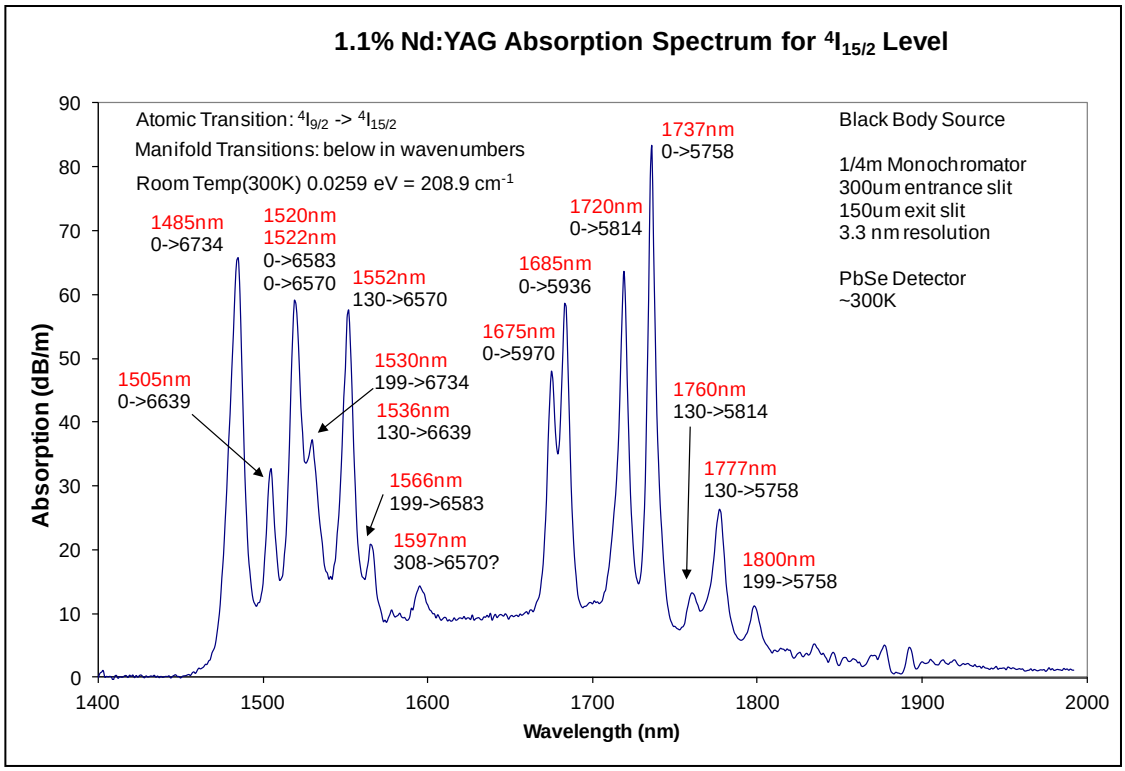

Figure 5-1: Optical absorption band for $^4I_{15/2}$ energy level in Nd:YAG

Level Scheme	Source 1	Wavelength	1st excited energy level	Source 2	Wavelength	2nd excited energy level
a	OPA -Signal	1485 nm-1520 nm	$^4I_{15/2}$ relaxes to $^4I_{11/2}$	Nd:YAG	1064 nm	$^4F_{3/2}$
b	OPA -Signal	1720 nm	$^4I_{15/2}$	Yb-Fiber	1112 nm	$^4F_{9/2}$
c	OPA -Idler	2254 nm	$^4I_{13/2}$	Yb-Fiber	1112 nm	$^4F_{7/2}$
d	OPA -Signal	1485 nm	$^4I_{15/2}$	OPA -Idler	1712 nm	$^4F_{5/2}$
d	OPA -Signal	1505 nm	$^4I_{15/2}$	OPA -Idler	1685 nm	$^4F_{5/2}$
d	OPA -Signal	1520 nm	$^4I_{15/2}$	OPA -Idler	1665 nm	$^4F_{5/2}$
d	OPA -Idler	1720 nm	$^4I_{15/2}$	OPA -Signal	1479 nm	$^4F_{5/2}$

Table 5-1: Experimental two-photon excitation schemes

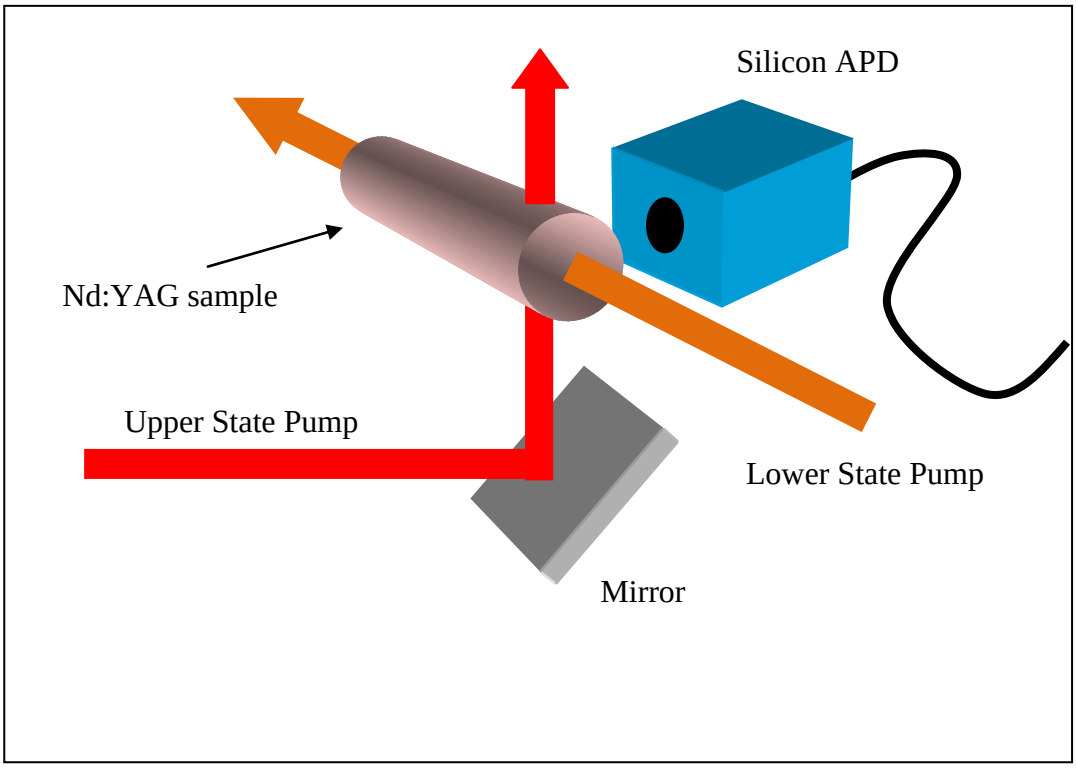

Figure 5-2: Diagram of sample setup for upconversion experiment

The high peak power of the Ti:Sapphire laser still easily caused nonlinear optical effects in the Nd:YAG substrate when used at full power. To avoid this problem the beam had to be attenuated down to an average power of approximately 8 mW. To estimate the potential detectability of the signal if upconversion was achieved a rough calculation was made. Based on the absorption peaks seen in Figure 5-1 it can be estimated that when the pump laser for the lower excited states is tuned to one of the absorption peaks the sample will approximately absorb the beam energy at 50 dB/m. If we assume that each pump beam is 2 mm in diameter and that they overlap in the sample, then in that space approximately 3% of the beam energy will be absorbed into the lower excited state. By dividing the power of the first pump laser by the quantum

energy of the pump photons and multiplying by the percentage of the energy absorbed we then determine the number of photons absorbed per second according to equation 5-1.

$$absorbed\ photons\ (1/\sec) = P * \frac{\lambda}{hc} \qquad (5\text{-}1)$$

Based on this calculation we find that about $19E^{15}$ atom/sec are excited to the $^4I_{15/2}$ level. If it is then assumed that the excited state absorption from the $^4I_{15/2}$ level happens at a similar rate of 3%, of the excited atoms in this case, and if we maintain that the second pump exceeds the power of the first pump source, then the number of atoms excited to the upper state should be approximately 3% of the previous number equaling $0.6E^{15}$ atoms/sec. At this point it should be noted that assuming any excited state absorption is a very big assumption. It is essentially the goal of this experiment to determine if there is any significant excited state absorption. Now based on some specifics of the detector size of 5 mm diameter and its placement 1 inch from the excitation spot, it can only pick up about 0.3% of the total possible signal. Additionally, only about 40% of the fluorescence will fall within the high quantum efficiency band of the silicon detector at 75%. To counter these limitations the silicon APD has a gain of approximately 100. By combining all of these numbers and by multiplying by the charge of an electron we can estimate the potential photocurrent from the detector.

$$Photocurrent = 0.6E^{15} * 0.003 * 0.4 * 0.75 * 100 * 1.6E^{-19}$$

$$Photocurrent = 9\ \mu A$$

A 9 μA photocurrent is certainly detectable. In the end this signal was not detected.

One additional test was run using the neodymium fiber sample with the 0.5% doping concentration. A Newport 10 mW CW 1.6 μm tunable laser diode was used in conjunction with a Navigator CW 1 watt Nd:YAG 1.064 μm. The output was monitored for emission as well as excited state absorption using an HP 71450B Optical Spectrum Analyzer. The Newport 1.6μm laser was switched on and off while leaving the Navigator 1.064 μm laser on. Using this technique a change in the monitored transmission of the 1.064 μm light through the fiber should have been detected if excited state absorption was present. Neither spontaneous emission nor excited state absorption was detected in this case.

Based on the measurements made in this study it appears that the transition probabilities going from the lower excited states to the upper states are extremely low. One of the reasons for this may be that the phonon relaxation down to the ground state is quite fast. This can be seen in the fact that the lower state lifetimes are on the order of 10 ns[17]. This factor should have been overcome with the test using CW lasers by keeping the lower state constantly populated. So what else could be preventing this process from working? It may be the fact that the upper energy levels prefer to transition to the lowest meta-stable state. This meta-stable state means that the transition probability from the upper states to the lower states is low. This may mean that the transition selection rules are preventing the reverse process from occurring as

well. However this was not an ideal experiment. It was hoped that the $^4I_{15/2}$ level could be excited, since it was accessible by laser sources that are available and is in the glass transmission window, and from there excite up to the upper energy levels. This is excitation scheme "b" and "d" in Table 5-1. The drawback here is that the reverse process has not been detected. All relaxation radiation has been to the lower three energy levels.

An alternative excitation scheme that was tried was to excite the fiber to the $^4I_{15/2}$, and assuming that it may relax down thru the $^4I_{13/2}$ and $^4I_{11/2}$ levels to the ground state, and excite it again from the $^4I_{11/2}$ up to the upper states. This is excitation schemes "a" and "c" in Table 5-1. The weakness in this idea is that the key process required for this to work has not been detected. It is not shown that the lower neodymium energy states relax in a cascading fashion thru each level.

I suggest that the properties that make neodymium a good rare-earth dopant for laser gain media may be what inhibits this material from being viable as the sensing medium in the proposed 2-photon upconversion scheme.

6 Conclusions and Future Work

The research presented in this thesis investigates the thermographic spectroscopy of Nd^{3+} doped silica fiber for potential use in a distributed temperature sensor. The fluorescence spectroscopy from several Nd-doped hosts was studied. The optical absorption spectra were measured and reported over the wavelength range from 400 nm to 2000 nm. These results show strong absorption around 590 nm for the upper states. While in the lower $^4I_{13/2}$ level the absorption was much weaker. Additionally, by inspection it is shown that the host material plays a strong role in the energy band structure of the neodymium doped material.

It was found that the neodymium doped materials radiatively relax in three primary bands from the $^4F_{3/2}$ level down to the $^4I_{9/2}$, $^4I_{11/2}$, and $^4I_{13/2}$ energy levels. The fluorescence lifetime and corresponding temperature coefficient of this lifetime was measured for two of the three transitions and additionally for two peaks within the $^4F_{3/2} \rightarrow {}^4I_{9/2}$ transition. It was found that the behavior was more consistent within a single energy level transition than between two different main transitions. For the two peaks within the $^4F_{3/2} \rightarrow {}^4I_{9/2}$ it was found that the emission exhibited very similar temperature coefficients at approximately -0.3 μs/°C while the nominal decay time of the fluorescence was somewhat different with 481 μs at 908 nm and 425 μs at 940 nm. While the energy transition $^4F_{3/2} \rightarrow {}^4I_{11/2}$ has a nominal decay of 520 μs and a positive temperature coefficient of 0.46 μs/°C. The behavior of this last result is consistent with Figure 4-1 and what was found for the 1.064 μm emission in Nd:YAG. However, the emission peak at 940nm appears to be the most linear with a temperature

coefficient of -0.26 μs/°C. Additionally it appears that this effect is caused by temperature dependent multi-phonon relaxation from the $^4F_{3/2}$ level to the ground state.

For the purpose of determining appropriate excitation scheme relatively high resolution absorption spectroscopy measurements were made. The range of energies covered in these measurements were from 23000cm^{-1} to 11000cm^{-1} for the upper excited states and for the $^4I_{15/2}$ lower excited state energies from 7100cm^{-1} to 5000cm^{-1}. It was found that the $^4I_{15/2}$ level lined up quite well with commercially available telecom laser wavelengths and had potential as an intermediate step in the 2-photon upconversion scheme. It was also determined that any excitation source of shorter wavelength than approximately 900 nm would excite the upper meta-stable state directly and not work for the 2-photon scheme.

While it was shown that the neodymium ion in silica glass did demonstrate some very useful thermographic properties it does have potential in the proposed upconversion distributed temperature sensor scheme. In the end 2-photon upconversion from the lower excited states was not demonstrated. It seems that the lack of results in this thesis does not definitively determine that upconversion from the lower excited states can't happen but that it is highly unlikely. It may also be that the properties, like a short lower state lifetime, that make Nd:YAG a good lasing material may indeed make it a poor choice for the type of sensor proposed in this thesis.

The following are a couple of suggestions for future studies. It is critical to find a material that exhibits the appropriate upconversion process with readily available laser sources.

1) **A study in multi-photon upconversion in rare earth materials both linear and nonlinear.** It may be found that a host doped with more than one rare-earth material can be made to provide upconversion in the laser source range necessary. A two-photon upconversion process has been demonstrated in Er:YALO[18] as well as in a host doped with both Pr^{3+} and Nd^{3+} [19]. Once the upconversion process can be established proper doping concentration will need to be determined for maximum signal generation while not reducing the properties of the material's temperature coefficient. Er:Silica has been shown to be excited by two-photon upconversion using photons in the 800 nm range. The drawback is that Erbium emits to the ground state strongly and can self excite. This behavior is why Erbium-doped fiber was not pursued however it may be useful to demonstrate the two photon upconversion process as a building block and to test laser diode driver technologies needed for this type of sensor.
2) **Determine a practical source excitation drive scheme.** Once an active optical fiber with the appropriate excitation and emission properties has been found it will be important to develop the timing based laser pulse generator. It is easy to say that a fiber will be spatially interrogated with a laser pulse over a short length but much harder to actually do. There are obviously lasers that

emit short pulses but they are typically large and expensive. If this sensor is to be a practical device it would likely need to be excited by laser diode sources being driven to emit sub-nanosecond pulses. There are a number of concepts that can be pursued. One way would be to directly control the length of each excitation laser pulse and where they overlap in the fiber. This method would also require that the lifetime of the excited energy levels be well understood and would likely set the final spatial resolution of the sensor. Another potential method that was proposed by S.W. Allison would be to sweep the fiber and for each increment of the length of fiber swept by the laser pulses, subtract off the previous signal leaving a new signal representing the new increment of excited fiber.

7 Bibliography

[1] S.W. Allison and G.T. Gillies, "Remote thermometry with thermographic phosphors: Instrumentation and applications", Rev. Sci. Instrum. 68(7), 2615 (1997)

[2] KTV. Grattan and Z.Y. Zhang, *Fiber Optic Fluorescence Thermometry* (Chapman and Hall, London, 1995), pg. 40

[3] P.F. Liao and H.P. Weber, "Fluorescence quenching of the $^4F_{3/2}$ state in Nd-doped yttrium aluminum garnet (YAG) by multiphonon relaxation", Journal of Applied Physics 45(7), 2931(1974)

[4] J. Ainslie, S.P. Craig, and S.T. Davey, "The Absorption and Fluorescence Spectra of Rare Earth Ions in Silica-Based Monomode Fiber", Journal of Lightwave Technology 6(2), 287 (1988)

[5] H. Kusama, O.J. Sovers, and T. Yoshioka, "Line Shift Method for Phosphor Temperature Measurements", Japanese Journal of Applied Physics 15, 2349 (1976)

[6] J. Selker, N. van de Giesen, M. Westhoff, W. Luxemburg, and M. Parlange, "Fiber optics opens the window on stream dynamics", Geophysical Research Letters 33, L24401 (2006)

[7] J. Gruber, M. Hills,T. Allik, C.K. Jayasankar, J. Quagliano, and F.S. Richardson, "Comparative analysis of Nd^{3+} ($4f^3$) energy levels in four garnet hosts", Physical Review B 41(12), 7999 (1990)

[8] G.H. Dieke and H.M. Crosswhite, "The Spectra of the Doubly and Triply Ionized Rare Earths", Applied Optics 2(7), 675 (1963)

[9] W.F. Krupke, "Radiative Transition Probabilities Within the $4f^3$ Ground Configuration of Nd:YAG", IEEE Journal of Quantum Electronics 7(4), 153 (1971)

[10] X. Bao, D.J. Webb, and D.A. Jackson, "22-km distributed temperature sensor using Brillouin gain in an optical fiber", Optics Letters 18(7), 552 (1993)

[11] M.C. Farries, M.E. Fermann, R.I. Laming, S.B. Poole, D.N. Payne, "Distributed Temperature Sensor Using Nd^{3+}-Doped Optical Fibre", Electronics Letters 22 (8), 418 (1986)

[12] S.W. Allison, T.J. McIntyre, L.C. Maxey, M.R. Cates, W.W. Manges, FreedomCar proposal: Fiber Optic Temperature Sensor for PEM Fuel Cells

[13] S.W. Allison, D.L. Beshears, and M.R. Cates, "A Wide-Range Phosphor Thermometry Technique", Oak Ridge National Laboratory, (1998)

[14] K.T.V. Grattan, J.D. Manwell, S.M.L. Sim, and C.A. Willson, "Lifetime investigation of fluorescence from neodymium-yttrium-aluminum garnet at elevated-temperature", Optics Communications 62(2), 104 (1987)

[15] S.A. Wade, S.F. Collins, and G.W. Baxter, "Fluorescence intensity ratio technique for optical fiber point temperature sensing", Journal of Applied Physics, 94(8), 4743(2003)

[16] S. B. Poole, D. N. Payne, R. J. Mears, M. E. Fermann, R. I. Laming, "Fabrication and Characterization of Low-Loss Optical Fibers Containing Rare-Earth Ions", Journal of Lightwave Technology LT-4(7), 870 (1986)

[17] F.E. Hovis, M. Stuff, C.J. Kennedy, B. Vivian, "Lower Level Relaxation of Nd:YAG", IEEE Journal of Quantum Electronics 28(1), 39 (1992)

[18] R. Scheps, "Upconversion Laser Processes", Prog. Quant. Electr. 20(4), 271 (1996)

[19] C.W. Struck and W.H. Fonger, "Thermal Quenching of Tb^{+3}, Tm^{+3}, Pr^{+3}, and Dy^{+3} $4f^n$ Emitting States in La_2O_2S", Journal of Applied Physics, 42(11), 4515(1971)

[20] K.W. Quoi, R.A. Lieberman, L.G. Cohen, D.S. Shenk, and J.R. Simpson, "Rare-Earth Doped Optical Fibers for Temperature Sensing", Journal of Lightwave Technology, 10(6), 847(1992)